Detection of different possible responses of a time-dependent nonlinear periodic chain with local and global potentials

Aurélie Labetoulle, Alireza Ture Savadkoohi, Emmanuel Gourdon

Detection of different possible responses of a time-dependent nonlinear periodic chain with local and global potentials

A. Labetoulle[a], A. Ture Savadkoohi[a], E. Gourdon[a]

[a]*ENTPE, École Centrale de Lyon, CNRS, LTDS, UMR5513, Vaulx-en-Velin Cedex, 69518, France*

Abstract

A time-dependent periodic chain of coupled nonlinear oscillators including local and global potentials is studied. The continuous form of system equations is projected on an arbitrary mode. Detection of different dynamics are highlighted leading to clarification of equilibrium and singular points of the reduced system. The analytical studies permit prediction/design of periodic and quasi-periodic regimes of the system validated by results obtained through direction numerical integrations.

Keywords: Nonlinear periodic chain, time-dependent, fast/slow dynamics, strongly modulated response

1. Introduction

Metamaterials are an assembly of mono- or multi-physics elements with architected arrangements which present extraordinary responses against induced excitations [1–3]. At their early stages, they were exploited in optics and electromagnetic fields [4, 5]. In the domain of mechanics, metamaterials are developed managing interesting characteristics of behavior at atomic and macro scales. These designed responses cover unusual mechanical properties in the macro scale such as zero or negative Poisson's ratio, density, mass and compressibility through the creation of bandgaps, where the system stops to respond or responds in controlled manner against external excitation or waves, or even to design localized energies and strains in materials [6–14]. One of special types of (meta) systems presenting unusual responses are chain of coupled oscillators which could be used to generate/design bandgaps [15–19], to localize energies or to exchange energies between modes [20–27]. Such designed systems can be applied for vibration control or energy harvesting [28–32]. Chain of oscillators can exploit different types of restoring forcing terms covering from cubic [33, 34] to Hertzian interactions [35] providing spatially localized waves in the chain leading to solitary waves and traveling breathers [36, 37]. Particles of a chain, in additions to global interactions with adjacent particles, can possess local potential as well [38]. For analyzing coupled nonlinear systems, several methods exist, including the harmonics balance method [19, 39, 40], averaging and multiple scale methods [41]. However, for our study for detection of different dynamics of the system, fast and slow dynamics, we use the complexification of Manevitch [42] accompanied by the multiple scale method [41]. These methods are particularly useful for studying both transient and permanent regimes [43]. The potential applications of this study are metamaterials in the mechanical or vibro-acoustic fields, for example by using nonlinear membranes[44].

In this work, we consider a periodic chain of oscillators possessing both local and global potentials. The local restoring forcing term is linear while the global one presents time-dependent cubic nonlinearity. This nonlinearity is unusual and is one of the novelties of this article. The behavior of unit cell of such chain has been already articulated by Labetoulle et al. [38]. The purpose of this article is to study the behavior of the chain. For this purpose, a reduced model of the discrete chain is defined, and analytical predictions of its behavior are developed based on parameters and external exication. The goal is to verify that these predictions can be applied to the chain. To this end, the dynamic

responses of the reduced system and of the chain are compared.. The organization of the paper is as follows: the general methodology for detection of different system dynamics based on projected continuous form of equations on an arbitrary mode is presented in Sect. 2. Then the developments are narrowed to consideration of cubic nonlinear restoring forcing function for the system with constant and time-dependent coefficients in Sects. 3 and 4, respectively. Several numerical results are provided in mentioned sections. Finally, the paper is concluded in Sect. 5.

2. General methodology

In this section, a system with general nonlinear stiffness will be presented and its different dynamics will be detected using analytical tools.

2.1. Problem statement

Let us consider a chain of coupled oscillators depicted in Fig. 1. It comprises L masses M_j where $j = 1, 2, ..., L$, equally spaced at the rest position with the distance Δx. These masses are coupled to each other by a linear stiffness and a damping denoted as k_1 and c_1, respectively. Each mass M_j is locally and linearly coupled an oscillators comprising a mass m_j, a pure odd nonlinear restoring forcing function denoted as $\Lambda(v)$ and a linear damping c_2. The displacements of masses M_j and m_j are denoted as u_j and v_j, respectively. Additionally, we assume that each mass M_j is subjected to external excitation, characterized by $F_j(t)$, and that $\frac{m_j}{M_j} \ll 1$. For this study, we assume that $M_j = M$

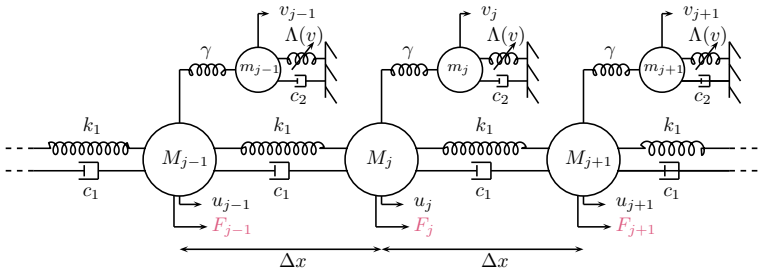

Figure 1: Diagram of the studied system: a chain of linearly coupled masses M_j which are locally and linearly coupled to masses m_j possessing a nonlinear restoring forcing function, where $j = 1, 2, .., L$. The M_j masses are equally spaced (Δx) at rest.

and $m_j = m$ for all $j = 1, 2, ..., L$. The governing equations of discrete system depicted in Fig. 1 are given by:

$$\begin{cases} M\dfrac{d^2u_j}{dt^2} + k_1(2u_j - u_{j+1} - u_{j-1}) + c_1\left(2\dfrac{du_j}{dt} - \dfrac{du_{j+1}}{dt} - \dfrac{du_{j-1}}{dt}\right) + \gamma(u_j - v_j) = F_j\sin(\Omega t) \\ m\dfrac{d^2v_j}{dt^2} + \Lambda(v) + c_2\dfrac{dv_j}{dt} + \gamma(v_j - u_j) = 0 \end{cases} \tag{1}$$

We define $X = (j-1)\Delta x = x\Delta x$ the continuous spatial variable where x is the normalized continuous spatial variable. Assuming that the number of cells L is very large ($L \gg 1$), we can approximate the displacements $u_j(t)$ and $v_j(t)$ as $u(x,t)$ and $v(x,t)$, respectively, where $x \in [0, L-1]$ and L becomes the length of the continuous system. Let us express the variables $u(x = j-1, t)$ and $v(x = j-1, t)$ in the form of Taylor series as described in [36]:

$$u_{(j\pm1,t)} = u_{(j-1,t)} \pm \frac{\partial u}{\partial x}(j-1,t) + ... + \frac{(\pm1)^n}{n!}\frac{\partial^n u}{\partial x^n}(j-1,t) + ... \tag{2}$$

$$v_{(j\pm1,t)} = v_{(j-1,t)} \pm \frac{\partial v}{\partial x}(j-1,t) + ... + \frac{(\pm1)^n}{n!}\frac{\partial^n v}{\partial x^n}(j-1,t) + ... \tag{3}$$

Consequently, the system can be expressed in the continuous domain, so Eq. (1) can be written as:

$$\begin{cases} M\dfrac{\partial^2 u(x,t)}{\partial t^2} - k_1\dfrac{\partial^2 u(x,t)}{\partial x^2} - c_1\dfrac{\partial}{\partial t}\left(\dfrac{\partial^2 u(x,t)}{\partial x^2}\right) + \gamma(u(x,t)-v(x,t)) = F(x)\sin(\Omega t) \\ m\dfrac{\partial^2 v(x,t)}{\partial t^2} + \Lambda(v(x,t)) + c_2\dfrac{\partial v(x,t)}{\partial t} + \gamma(v(x,t)-u(x,t)) = 0 \end{cases} \tag{4}$$

In the next subsection, modal characteristics of the obtained continuous system described in Eq. (4) will be analyzed.

2.2. Determination of linear modes of the continuous system

To detect the modal characteristics of presented system in Fig. 1, we focus on the linear and conservative elements of Eq. (4) which can be expressed as:

$$\begin{cases} M\dfrac{\partial^2 u(x,t)}{\partial t^2} - k_1\dfrac{\partial^2 u(x,t)}{\partial x^2} + \gamma(u(x,t)-v(x,t)) = 0 \\ m\dfrac{\partial^2 v(x,t)}{\partial t^2} + \gamma(v(x,t)-u(x,t)) = 0 \end{cases} \tag{5}$$

The spatio-temporal variables of Eq. (5) are separated as follows:

$$\begin{cases} u(x,t) = A(x)e^{i\omega t} \\ v(x,t) = D(x)e^{i\omega t} \end{cases} \tag{6}$$

where ω represents the angular frequency of the continuous system. After injecting Eq. (6) into Eq. (5), we obtain:

$$\begin{cases} (-M\omega^2+\gamma)A(x) - k_1\dfrac{d^2A(x)}{dx^2} - \gamma D(x) = 0 \\ (-m\omega^2+\gamma)D(x) - \gamma A(x) = 0 \end{cases} \tag{7}$$

Thus, we can write:

$$D(x) = \lambda A(x) \tag{8}$$

with

$$\lambda = \frac{\gamma}{-\omega^2 m + \gamma} \tag{9}$$

The first equation of the Eq. (7) can be reorganized as:

$$\frac{d^2A(x)}{dx^2} + \underbrace{\frac{1}{k_1}\left(M\omega^2 - \gamma + \frac{\gamma^2}{-\omega^2 m+\gamma}\right)}_{\mu^2} A(x) = 0 \tag{10}$$

Considering a periodic chain with the same displacement and rotation for the first and last cells as the boundary conditions, the non-trivial solutions of Eq. (10) are:

$$A_k(x) = \alpha\cos(\mu_k x) \tag{11}$$

with

$$\mu_k = \frac{2k\pi}{L} \tag{12}$$

where $k \in \mathbb{N}^+$ is the mode number. To determine α, we opt for the normalized form of $A_k(x)$ leading to, $\alpha = \sqrt{\frac{2}{L}}$. Then, the spatio-temporal system variables can be expressed as:

$$\begin{cases} u(x,t) = \sum_k A_k(x) g_k(t) \\ v(x,t) = \sum_k \lambda_k A_k(x) \eta_k(t) = \sum_k A_k(x) h_k(t) \end{cases} \tag{13}$$

where $g_k(t)$ and $h_k(t)$ represent the modal coordinates of the continuous system. To investigate behaviors around a spacial mode, the continuous system will be arbitrarily projected on one of its linear modes and further treatments will be carried out on it.

2.3. Projection of the continuous system on the k^{th} mode

We aim to study the projected form of continuous system equations on its k^{th} mode, i.e. $A_k(x)$. To this end, we apply the inner product between system equations and the function $A_k(x)$. The inner product on the vector space of general continuous functions $f(s)$ and $g(s)$ in the interval $[a, b]$ is given by:

$$\langle f(s)\ ,\ g(s) \rangle = \int_a^b f(s) g(s)\, ds \tag{14}$$

In applying Eq. (14), we assume that the response of the continuous system is dominated by the k^{th} mode and we ignore internal resonances and mode couplings of the system. Then, from Eq. (13) we can write:

$$\begin{cases} u(x,t) = A_k(x) g_k(t) \\ v(x,t) = A_k(x) h_k(t) \end{cases} \tag{15}$$

Then the projection of Eq. (4) on $A_k(x)$ reads:

$$\begin{cases} M \dfrac{d^2 g_k(t)}{dt^2} + k_1 \mu_k^2 g_k(t) + c_1 \mu_k^2 \dfrac{\partial g_k(t)}{dt} + \gamma \left(g_k(t) - h_k(t) \right) = \displaystyle\int_0^L F(x) \sin(\Omega t) A_k(x) dx \\ m \dfrac{d^2 h_k(t)}{dt^2} + \displaystyle\int_0^L \Lambda(v) A_k(x)\, dx + c_2 \dfrac{dh_k(t)}{dt} + \gamma \left(h_k(t) - g_k(t) \right) = 0 \end{cases} \tag{16}$$

For the rest of this paper and for simplicity, the index k will be dropped from modal coordinates $g_k(t)$, $h_k(t)$ and μ_k. The equations of the continuous system projected on the k^{th} mode, as presented in Eq. (16), are similar to a two degree-of-freedom (dof) system (see Fig. 2). This system consists of a mass M with the modal displacement $g(t)$ linearly coupled to a mass m with the modal coordinate as $h(t)$ with a nonlinear restoring forcing function [38]. In the following, this system is referred to as the reduced system or continuous system in the modal domain. The objective is to identify the fast and slow dynamics of this system in order to predict its behavior. For this purpose, the governing equations are non-dimensionalized (a new time τ is defined), then the complex variables of Manevitch [42] are introduced and the Galerkin method is used to keep the first harmonic of the system.

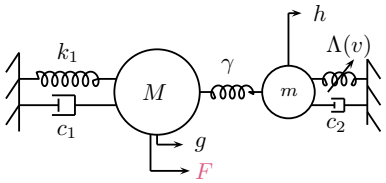

Figure 2: Schematic of the reduced system: a main mass M is linearly coupled to a mass m possessing nonlinear restoring forcing function. The displacements of M and m are noted as $g(\tau)$ and $h(\tau)$, respectively.

2.4. Detection of different dynamics of the reduced system

2.4.1. Non-dimensionalization and complexification of the reduced system

We introduce a new time $\tau_k = t\omega_k$, where ω_k is the angular frequency of the k$^{\text{th}}$ mode of the continuous system. In the following the index of the non-dimensionalized time τ_k is dropped for simplicity. Thus, Eq. (16) is written as follows:

$$\begin{cases} \dfrac{d^2g(\tau)}{d\tau^2} + \dfrac{k_1\mu^2}{M\omega^2}g(\tau) + \varepsilon\dfrac{c_1\mu^2}{\omega M}\dfrac{dg(\tau)}{d\tau} + \varepsilon\dfrac{\gamma}{M\omega^2}\left(g(\tau) - h(\tau)\right) = \sin(\nu\tau)\displaystyle\int_0^L \frac{F(x)}{\omega^2 M}A_k(x)dx \\ \varepsilon\dfrac{d^2h(\tau)}{d\tau^2} + \dfrac{1}{\omega^2 M}\displaystyle\int_0^L \Lambda(v)A_k(x)dx + \varepsilon\dfrac{c_2}{\omega M}\dfrac{dh(\tau)}{d\tau} + \varepsilon\dfrac{\gamma}{M\omega^2}\left(h(\tau) - g(\tau)\right) = 0 \end{cases} \tag{17}$$

with $\varepsilon = \frac{m}{M} \ll 1$ and $\nu = \frac{\Omega}{\omega}$, where ω represents the mode of the continuous system that depends on μ according to Eq. (10) (at the order 1, $\omega^2 = \frac{\mu^2 k_1}{M}$). The simplified form of Eq. (17) is given by:

$$\begin{cases} \dfrac{d^2g(\tau)}{d\tau^2} + g(\tau) + \varepsilon\mu z_1\dfrac{dg(\tau)}{d\tau} + \varepsilon\dfrac{X_0}{\mu^2}\left(g(\tau) - h(\tau)\right) = \varepsilon\sin(\nu\tau)\displaystyle\int_0^L \frac{F_0(x)}{\alpha\mu^2}A_k(x)dx \\ \varepsilon\dfrac{d^2h(\tau)}{d\tau^2} + \varepsilon\Lambda_1(v) + \varepsilon\dfrac{z_2}{\mu_k}\dfrac{dh(\tau)}{d\tau} + \varepsilon\dfrac{X_0}{\mu^2}\left(h(\tau) - g(\tau)\right) = 0 \end{cases} \tag{18}$$

with $\varepsilon z_1 = \dfrac{c_1}{\sqrt{k_1 M}}$, $\varepsilon X_0 = \dfrac{\gamma}{k_1}$, $\varepsilon\dfrac{F_0(x)}{\alpha} = \dfrac{F(x)}{k_1}$, $\varepsilon\Lambda_1 = \dfrac{1}{\mu_k^2 k_1}\displaystyle\int_0^L \Lambda(v)A_k(x)dx$, $\varepsilon z_2 = \dfrac{c_2}{\sqrt{k_1 M}}$. Assuming $F(x)$ follows the linear mode of the continuous system with $F(x) = F\alpha\cos(\mu x))$, then we can define: $\varepsilon\sin(\nu\tau)\displaystyle\int_0^L \frac{F_0(x)}{\alpha\mu^2}A_k(x)dx = \varepsilon\frac{F_0}{\alpha\mu^2}\sin(\nu\tau)$. In order to detect different dynamics of the systems, following the complex variables of Manevitch are introduced:

$$\begin{cases} \varphi_{1CM}e^{i\nu\tau} = \dot{g}(\tau) + i\nu g(\tau) \\ \varphi_{2CM}e^{i\nu\tau} = \dot{h}(\tau) + i\nu h(\tau) \end{cases} \tag{19}$$

with $i^2 = -1$. Then, a multiple scale method [41] is applied, where the time τ is decomposed into fast ($\tau_0 = \tau$) and slow time scales ($\tau_p = \varepsilon^p\tau$, $p = 1, 2, ...$). Consequently, we obtain:

$$\frac{d}{d\tau} = \frac{\partial}{\partial\tau_0} + .. + \varepsilon^p\frac{\partial}{\partial\tau_p} \tag{20}$$

Solutions can be expressed in the terms of Fourier series, and a Galerkin method is used to keep the first harmonic of the system and truncate others [45, 46]. For an arbitrary function $s(\varphi_{1CM}, \varphi_{2CM}, \varphi^*_{1CM}, \varphi^*_{2CM})$, the expression corresponding to the first harmonic is denoted as S:

$$S(\varphi_{1CM}, \varphi_{2CM}, \varphi^*_{1CM}, \varphi^*_{2CM}) = \frac{\nu}{2\pi}\int_0^{\frac{2\pi}{\nu}} s(\varphi_{1CM}, \varphi_{2CM}, \varphi^*_{1CM}, \varphi^*_{2CM})e^{-1i\nu\tau}d\tau \tag{21}$$

Thus, Eq. (18) becomes:

$$\begin{cases} \dot{\varphi}_{1CM} + \dfrac{i\nu}{2}\varphi_{1CM} + \dfrac{1}{2i\nu}\varphi_{1CM} + \varepsilon\dfrac{z_1\mu\varphi_{1CM}}{2} + \varepsilon\dfrac{X_0}{2i\nu\mu^2}(\varphi_{1CM} - \varphi_{2CM}) = \dfrac{\varepsilon}{2i\alpha\mu^2}\displaystyle\int_0^L F_0(x)A_k(x)dx \\ \varepsilon\left(\dot{\varphi}_{2CM} + \dfrac{i\nu}{2}\varphi_{2CM} + \dfrac{z_2}{2\mu}\varphi_{2CM} + \dfrac{X_0}{2i\nu\mu^2}(\varphi_{2CM} - \varphi_{1CM}) + G(v)\right) = 0 \end{cases} \tag{22}$$

with $G(v) = \dfrac{\nu}{2\pi}\displaystyle\int_0^{\frac{2\pi}{\nu}} \Lambda_1(v)e^{-i\nu\tau}d\tau$. We aim to clarify the system behaviors around the $1:1$ resonance. To achieve this, we set $\nu = 1 + \varepsilon\sigma$. If we consider $F(x) = \alpha\cos(\mu x)$, we obtain:

$$\frac{\varepsilon}{2i\alpha\mu^2}\int_0^L F_0(x)A_k(x)dx = \frac{\varepsilon F_0}{2i\alpha\mu^2} \tag{23}$$

In the following sections we will examine the equations of the reduced system at different orders of ε to detect different dynamics.

2.4.2. Fast dynamics

Let us consider ε^0 order of the Eq. (22):

$$\begin{cases} \dfrac{\partial\varphi_{1CM}}{\partial\tau_0} = 0 \\ \dfrac{\partial\varphi_{2CM}}{\partial\tau_0} + \mathscr{H}(\varphi_{1CM}, \varphi_{2CM}) = 0 \end{cases} \tag{24}$$

with,

$$\mathscr{H} = \left(\frac{i}{2} + \frac{z_2}{2\mu} - \frac{iX_0}{2\mu^2}\right)\varphi_{2CM} + \frac{iX_0}{2\mu^2}\varphi_{1CM} + G(v) \tag{25}$$

At order ε^0, $\dfrac{\partial\varphi_{1CM}}{\partial\tau_0} = 0$ is satisfied. Since $\tau_0 \to +\infty$, i.e. in an asymptotic state, we have $\dfrac{\partial\varphi_{2CM}}{\partial\tau_0} = 0$, leading to $\mathscr{H}(\varphi_{1CM}, \varphi_{2CM}) = 0$, which is called the Slow Invariant Manifold (SIM) of the system. Let us consider the complex variables of Manevitch (Eq. (19)) in the polar domain:

$$\begin{cases} \varphi_{1CM} = N_{1CM}e^{i\delta_{1CM}} \\ \varphi_{2CM} = N_{2CM}e^{i\delta_{2CM}} \end{cases} \tag{26}$$

with $N_{qCM} \in \mathbb{N}^+$ and $\delta_{qCM} \in \mathbb{R}$, $q = 1, 2$.

2.4.3. Slow dynamics

In this section, we aim to identify the characteristic points of the system, i.e. the equilibrium and singular points. To this end, we will search for the ε^1 order of Eq. (22). The first equation of Eq. (22) at the ε^1 order is:

$$\frac{\partial\varphi_{1CM}}{\partial\tau_1} + \underbrace{\frac{i\sigma}{2}\varphi_{1CM} + \frac{i\sigma}{2}\varphi_{1CM} + \frac{\mu z_1}{2}\varphi_{1CM} - \frac{iX_0}{2\mu^2}(\varphi_{1CM} - \varphi_{2CM}) + \frac{iF_0}{2\alpha\mu^2}}_{\mathscr{E}} = 0 \tag{27}$$

The evolution of the SIM (see Eq. (25)) is studied at the slow time scale τ_1, by denoting the complex conjugate of variables by $(.)^*$, we have in matrix form:

$$\underbrace{\begin{bmatrix} \dfrac{\partial \mathscr{H}}{\partial \varphi_{2CM}} & \dfrac{\partial \mathscr{H}}{\partial \varphi^*_{2CM}} \\ \dfrac{\partial \mathscr{H}^*}{\partial \varphi_{2CM}} & \dfrac{\partial \mathscr{H}^*}{\partial \varphi^*_{2CM}} \end{bmatrix}}_{\mathbb{B}} \begin{bmatrix} \dfrac{\partial \varphi_{2CM}}{\partial \tau_1} \\ \dfrac{\partial \varphi^*_{2CM}}{\partial \tau_1} \end{bmatrix} = - \begin{bmatrix} \dfrac{\partial \mathscr{H}}{\partial \varphi_1} & \dfrac{\partial \mathscr{H}}{\partial \varphi^*_1} \\ \dfrac{\partial \mathscr{H}^*}{\partial \varphi_1} & \dfrac{\partial \mathscr{H}^*}{\partial \varphi^*_1} \end{bmatrix} \begin{bmatrix} \dfrac{\partial \varphi_{1CM}}{\partial \tau_1} = -\mathscr{E} \\ \dfrac{\partial \varphi^*_{1CM}}{\partial \tau_1} = -\mathscr{E}^* \end{bmatrix} \tag{28}$$

Thus, equilibrium points can be defined as the points that satisfy the following conditions:

$$\begin{cases} \mathscr{E}(\varphi_{1CM}, \varphi_{2CM}, \varphi^*_{1CM}, \varphi^*_{2CM}) = 0 \\ \mathscr{H}(\varphi_{1CM}, \varphi_{2CM}, \varphi^*_{1CM}, \varphi^*_{2CM}) = 0 \\ \det(\mathbb{B}) \neq 0 \end{cases} \tag{29}$$

and the singular points are defined such as:

$$\begin{cases} \mathscr{E}(\varphi_{1CM}, \varphi_{2CM}, \varphi^*_{1CM}, \varphi^*_{2CM}) = 0 \\ \mathscr{H}(\varphi_{1CM}, \varphi_{2CM}, \varphi^*_{1CM}, \varphi^*_{2CM}) = 0 \\ \det(\mathbb{B}) = 0 \end{cases} \tag{30}$$

Here the equilibrium and singular points are defined. In the next subsection, some preliminary treatments of the discrete form of the system equations are carried out. Then, the results obtained from the reduced system are confronted with those of the discrete equations.

2.5. Discrete system

Let us non-dimensionalize the discrete equations of the chain (see Eq. (1)) by considering $F_j = \alpha F \cos(\mu(j-1))$, so we have:

$$\begin{cases} M\dfrac{d^2u_j}{dt^2} + k_1(2u_j - u_{j+1} - u_{j-1}) + c_1\left(2\dfrac{du_j}{dt} - \dfrac{du_{j+1}}{dt} - \dfrac{du_{j-1}}{dt}\right) \\ \qquad +\gamma(u_j - v_j) = \alpha F \cos(\mu(j-1))\sin(\Omega t) \\ \\ m\dfrac{d^2v_j}{dt^2} + \Lambda(v) + c_2\dfrac{dv_j}{dt} + \gamma(v_j - u_j) = 0 \end{cases} \tag{31}$$

After introducing the same time as for the reduced system: $\tau = t\omega$, considering $\omega^2 = \dfrac{k_1\mu^2}{M}$ at the order $O(1)$, and introducing the parameters of Eq. (18), Eq. (31) becomes:

$$\begin{cases} \dfrac{d^2u_j}{d\tau^2} + \dfrac{1}{\mu^2}(2u_j - u_{j+1} - u_{j-1}) + \dfrac{\varepsilon z_1}{\mu}\left(2\dfrac{du_j}{d\tau} - \dfrac{du_{j+1}}{d\tau} - \dfrac{du_{j-1}}{d\tau}\right) + \\ \qquad \dfrac{\varepsilon X_0}{\mu^2}(u_j - v_j) = \dfrac{\varepsilon F_0}{\mu^2}\cos(\mu(j-1))\sin(\nu\tau) \\ \\ \varepsilon\dfrac{d^2v_j}{d\tau^2} + \dfrac{\Lambda(v)}{k_1\mu^2} + \dfrac{\varepsilon z_2}{\mu}\dfrac{dv_j}{d\tau} + \dfrac{\varepsilon X_0}{\mu^2}(v_j - u_j) = 0 \end{cases} \tag{32}$$

Furthermore, we assume that the discrete system is under initial conditions that follow the k^{th} modal form of the chain (see Eq. (11) and 13) i.e.: $u_j(\tau = 0) = \alpha\cos(\mu_k(j-1))g(\tau = 0)$, and $v_j(\tau = 0) = \alpha\cos(\mu_k(j-1))h(\tau = 0)$, where $j = 1, 2, .., L$, $g(\tau = 0)$ and $h(\tau = 0)$ are the initial modal coordinates of the reduced system.

2.6. Comparison of results obtained from discrete and reduced systems

Two methods are used to compare the behavior of the discrete and reduced systems. In the first one, the numerical results obtained from the discrete form of equations are projected on the k$^{\text{th}}$ linear mode of the continuous system defined in Eq. (11) $A_k(x) = \alpha\cos(\mu_k x)$ where x is the position of the cells and $x = j-1$ with $j = 1, ..., L$. We set $\underline{\mathbf{A}}_{kD}$ as follows:

$$\underline{\mathbf{A}}_{kD} = \begin{pmatrix} \alpha\cos(\mu_k \times 0) \\ \vdots \\ \alpha\cos(\mu_k \times (j-1)) \\ \vdots \\ \alpha\cos(\mu_k \times (L-1)) \end{pmatrix} \tag{33}$$

We also define $\underline{\mathbf{U}}$, $\underline{\dot{\mathbf{U}}}$, $\underline{\mathbf{V}}$ and $\underline{\dot{\mathbf{V}}}$ as the displacement and velocity vectors of the masses M_j and m_j, respectively:

$$\underline{\mathbf{U}} = \begin{pmatrix} u_1(\tau) \\ \vdots \\ u_j(\tau) \\ \vdots \\ u_L(\tau) \end{pmatrix} ; \underline{\dot{\mathbf{U}}} = \begin{pmatrix} \dot{u}_1(\tau) \\ \vdots \\ \dot{u}_j(\tau) \\ \vdots \\ \dot{u}_L(\tau) \end{pmatrix} ; \underline{\mathbf{V}} = \begin{pmatrix} v_1(\tau) \\ \vdots \\ v_j(\tau) \\ \vdots \\ v_L(\tau) \end{pmatrix} ; \underline{\dot{\mathbf{V}}} = \begin{pmatrix} \dot{v}_1(\tau) \\ \vdots \\ \dot{v}_j(\tau) \\ \vdots \\ \dot{v}_L(\tau) \end{pmatrix} \tag{34}$$

Moreover, we set $g_D(\tau)$, $h_D(\tau)$, $\dot{g}_D(\tau)$ and $\dot{h}_D(\tau)$ as the modal displacements and velocities associated with the masses M and m obtained from the discrete system, and they are defined as:

$$\begin{cases} g_D(\tau) = \underline{\mathbf{A}}_{kD}^T \underline{\mathbf{U}}(\tau) \\ h_D(\tau) = \underline{\mathbf{A}}_{kD}^T \underline{\mathbf{V}}(\tau) \\ \dot{g}_D(\tau) = \underline{\mathbf{A}}_{kD}^T \underline{\dot{\mathbf{U}}}(\tau) \\ \dot{h}_D(\tau) = \underline{\mathbf{A}}_{kD}^T \underline{\dot{\mathbf{V}}}(\tau) \end{cases} \tag{35}$$

Thus, results of the system in the modal domain obtained from discrete system (discrete system in the modal domain) and the reduced system can be compared. The second method consists of calculating the response of the continuous domain from the response of the reduced system. In other words, $u(x,t)$, $v(x,t)$ and their derivatives are calculated from $g(t)$, $h(t)$ and their derivatives using Eq. (15). The numerical results obtained in the physical domain from the reduced system are then compared with those of the discrete chain. Both methods are summarized in Fig. 3.

Let us introduce the complex variables of Manevitch for the different cases: the reduced system denoted as φ_{qCM} (see Eq. (19)), the continuous system in the physical domain as φ_{qCMPh}, the discrete system as φ_{qDPh} and the discrete system in the modal domain as φ_{qDM}, where $q = 1, 2$.

$$\begin{cases} \varphi_{1CMPh} e^{i\nu\tau} = \dot{u}(x,\tau) + i\nu u(x,\tau) = A_k(x)\dot{g}(\tau) + i\nu A_k(x) g(\tau) = A_k(x)\varphi_{1CM} e^{i\nu\tau} \\ \\ \varphi_{2CMPh} e^{i\nu\tau} = \dot{v}(x,\tau) + i\nu v(x,\tau) = A_k(x)\dot{h}(\tau) + i\nu A_k(x) h(\tau) = A_k(x)\varphi_{2CM} e^{i\nu\tau} \end{cases} \tag{36}$$

$$\begin{cases} \varphi_{1DPh,j} e^{i\nu\tau} = \dot{u}_j(\tau) + i\nu u_j(\tau) \\ \varphi_{2DPh,j} e^{i\nu\tau} = \dot{v}_j(\tau) + i\nu v_j(\tau) \end{cases} \tag{37}$$

$$\begin{cases} \varphi_{1DM} e^{i\nu\tau} = \dot{g}_D(\tau) + i\nu g_D(\tau) \\ \varphi_{2DM} e^{i\nu\tau} = \dot{h}_D(\tau) + i\nu h_D(\tau) \end{cases} \tag{38}$$

In the polar domain, for $q = 1, 2$:

$$\varphi_{qCMPh} = N_{qCMPh} e^{i\delta_{qCMPh}} \tag{39}$$

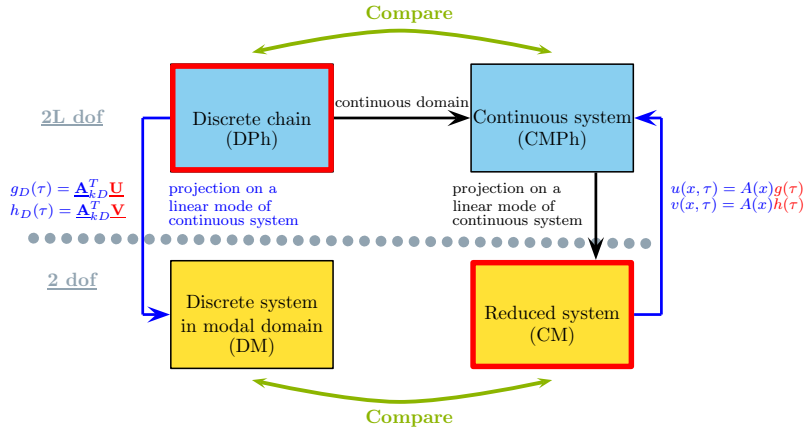

Figure 3: Diagram summarizing the methodology used to compare results obtained from discrete and reduced systems. Elements in red are the result of numerical integrations.

	dof	notation	N_q	δ_q
Continuous system, Modal (1)	2	$g(t)$, $h(\tau)$	N_{qCM}	δ_{qCM}
Continuous system, physical (2)	2L	$u(x,\tau)$, $v(x,\tau)$	N_{qCMPh}	δ_{qCMPh}
Discrete system, Modal (3)	2	$g_D(t)$, $h_D(\tau)$	N_{qDM}	δ_{qDM}
Discrete chain, Physical (4)	2L	$u_j(\tau)$, $v_j(\tau)$	N_{qDPh}	δ_{qDPh}

Table 1: Notation of the different chains. (1): modal domain obtained from continuous system (reduced system); (2): physical domain obtained from the modal domain of continuous system; (3): modal domain obtained from the discrete system; (4): physical domain from the discrete system ($q = 1, 2$).

$$\varphi_{qDPh,j} = N_{qDPh,j} e^{i\delta_{qDPh,j}} \tag{40}$$

$$\varphi_{qDM} = N_{qDM} e^{i\delta_{qDM}} \tag{41}$$

For clarity, the different notations are summarized in Table 1.

In summary, in this section, a reduced system (2 dof) was defined from the discrete system (2L dof) by writing the equations in the continuous domain and then by projecting them on an arbitrary linear mode of the continuous system. Analytical studies were performed to predict the behavior of the reduced system. Finally, two comparison methods were presented to verify that the reduced system is representative of the discrete one.
In the following sections, the general methodology developed in Sect. 2 will be applied for a system with a constant cubic stiffness (see Sect. 3) and then for a system with time-dependent cubic stiffness (see Sect. 4).

3. Presentation of the system possessing a constant cubic nonlinear stiffness

In this section, we will consider the discrete and reduced systems with constant stiffness. The methodology explained in Sect. 2 will be employed to study different dynamics of the reduced system.

3.1. General presentation

Let us assume that the nonlinear restoring forcing function $\Lambda(v)$ (see Fig. 1 and Eq. (1)) is cubic.

$$\Lambda(v) = k_2 v_j^3(t) \tag{42}$$

where k_2 is the stiffness of the nonlinear oscillators. In the continuous domain $\Lambda(v)$ reads:

$$\Lambda(v) = k_2 v^3(x,t) = k_2 A_k(x)^3 h_k(t)^3 \tag{43}$$

Considering the continuous system in the modal domain $\int_0^L \Lambda(v) A_k(x)\, dx$ as defined in Eq. (16) reads:

$$\int_0^L \Lambda(v) A_k(x)\, dx = k_2 h(t)^3 \int_0^L A_k(x)^3 A_k(x)\, dx = \frac{3}{2}\frac{k_2 h(t)^3}{L} \tag{44}$$

The non-dimensionalized equations of the continuous system in the modal domain (Eq. (17)) becomes:

$$\begin{cases} \dfrac{d^2 g(\tau)}{d\tau^2} + g(\tau) + \varepsilon\mu z_1 \dfrac{dg(\tau)}{d\tau} + \varepsilon \dfrac{X_0}{\mu^2}\left(g(\tau) - h(\tau)\right) = \varepsilon \sin(\nu\tau) \displaystyle\int_0^L \frac{F_0(x)}{\alpha\mu^2} A_k(x) dx \\ \varepsilon \dfrac{d^2 h(\tau)}{d\tau^2} + \varepsilon \dfrac{3}{2L}\dfrac{P_0}{\mu^2} h(\tau)^3 + \varepsilon \dfrac{z_2}{\mu}\dfrac{dh(\tau)}{d\tau} + \varepsilon \dfrac{X_0}{\mu^2}\left(h(\tau) - g(\tau)\right) = 0 \end{cases} \tag{45}$$

with $\varepsilon P_0 = \dfrac{k_2}{k_1}$. Then the complex variables of Manevitch are introduced. For better readability, φ_{qCM}, N_{qCM} are denoted as φ_q and N_q, with $q = 1, 2$ for the analytical developments. After applying the Galerkin technique, Eq. (22) becomes:

$$\begin{cases} \dot{\varphi_1} + \dfrac{i\nu}{2} + \dfrac{1}{2i\nu}\varphi_1 + \varepsilon\dfrac{z_1\mu\varphi_1}{2} + \varepsilon\dfrac{X_0}{2i\nu\mu^2}(\varphi_1 - \varphi_2) = \dfrac{\varepsilon F_0}{2i\alpha\mu^2} \\ \varepsilon\left(\dot{\varphi_2} + \dfrac{i\nu}{2}\varphi_2 - \dfrac{9P_0}{16\nu^3\mu^2 L} i\varphi_2|\varphi_2|^2 + \dfrac{z_2}{2\mu}\varphi_2 + \dfrac{X_0}{2i\nu\mu^2}(\varphi_2 - \varphi_1)\right) = 0 \end{cases} \tag{46}$$

In the next subsection, several system dynamics will be clarified as explained in Sect. 2.

3.2. Detection of different dynamics of reduced system

3.2.1. Fast dynamics

To detect the fast dynamics of the reduced system, Eq. (46) is considered at the order ε^0. Then, $\dfrac{\partial\varphi_1}{\partial\tau_0} = 0$ is verified and we seek an asymptotic state, i.e. $\tau_0 \to \infty$ so $\dfrac{\partial\varphi_2}{\partial\tau_0} = 0$. Thus, as defined in Eq. (24), we look for $\mathscr{H}(\varphi_1, \varphi_2) = 0$ with:

$$\mathscr{H} = \frac{\varphi_2}{2}\left(i + \frac{z_2}{\mu} - i\frac{X_0}{\mu^2} - \frac{9iP_0}{8L\mu^2}|\varphi_2|^2\right) + \frac{iX_0\varphi_1}{2\mu^2} \tag{47}$$

The equation of the SIM of the reduced system, with the polar variables $\varphi_q = N_q e^{i\delta_q}$ $(q = 1, 2)$, is in the real domain:

$$N_1 = \frac{N_2}{X_0}\sqrt{(z_2\mu)^2 + \left(\mu^2 - X_0 - \frac{9P_0}{8L}N_2^2\right)^2} \tag{48}$$

Now, we would like to determine the stability limits of the SIM. To do this, φ_2 and φ_2^* are linearly perturbed:

$$\begin{cases} \varphi_2 \to \varphi_2 + \Delta\varphi_2, & |\Delta\varphi_2| \ll |\varphi_2| \\ \varphi_2^* \to \varphi_2^* + \Delta\varphi_2^*, & |\Delta\varphi_2^*| \ll |\varphi_2^*| \end{cases} \tag{49}$$

where $(\cdot)^*$ stands for complex conjugate of the complex variable. After substituting Eq. (49) into the second equation of Eq. (46) at the order ε^0 (and also into its complex conjugate), the following system is obtained:

$$\begin{pmatrix} \frac{\partial \Delta\varphi_2}{\partial \tau_0} \\ \frac{\partial \Delta\varphi_2^*}{\partial \tau_0} \end{pmatrix} = \underbrace{\frac{1}{2}\begin{pmatrix} -i\left(1-\frac{X_0}{\mu^2}-\frac{9}{4}N_2^2\right)-\frac{z_2}{\mu} & \frac{9}{8L\mu^2}iP_0\varphi_2^2 \\ -\frac{9}{8L\mu^2}iP_0\varphi_2^{2*} & i\left(1-\frac{X_0}{\mu^2}-\frac{9}{4}N_2^2\right)-\frac{z_2}{\mu} \end{pmatrix}}_{\mathbb{M}} \begin{pmatrix} \Delta\varphi_2 \\ \Delta\varphi_2^* \end{pmatrix} \tag{50}$$

To study the stability of the SIM, the eigenvalues of the matrix $\mathbb{M}$, denoted as $\lambda_{\mathbb{M}}$ are evaluated. To find the unstable zone of the SIM, we search for the characteristic equation of the matrix $\mathbb{M}$, which is expressed as follows:

$$\lambda_{\mathbb{M}}^2 - \alpha_{\mathbb{M}}\lambda_{\mathbb{M}} + \beta_{\mathbb{M}} = 0 \tag{51}$$

By noting $\lambda_{\mathbb{M},1}$ and $\lambda_{\mathbb{M},2}$ as the solutions of Eq. (51), we have $\lambda_{\mathbb{M},1} + \lambda_{\mathbb{M},2} = \alpha_{\mathbb{M}} = -\frac{z_2}{\mu}$ and $\lambda_{\mathbb{M},1}\lambda_{\mathbb{M},2} = \beta_{\mathbb{M}}$. The system is unstable if the real parts of $\lambda_{\mathbb{M},1}$ and $\lambda_{\mathbb{M},2}$ are positive, i.e. $\beta_{\mathbb{M}} \geq 0$. Thus, the equation $\beta_{\mathbb{M}} = 0$ corresponds to the stability boundary of the SIM, defined as:

$$\frac{243}{64}\frac{P_0^2}{L^2}N_2^4 - \frac{9}{2}(\mu^2 - X_0)\frac{P_0}{L}N_2^2 + (\mu^2 - X_0)^2 + (z_2\mu)^2 = 0 \tag{52}$$

Figure 4 shows an example of the SIM for provided parameters from Table 2 for the first mode of the chain, while Figs. 5a and 5b depict the SIM for the third and tenth modes with the unstable zone in green. For simplicity, N_{qCM} is denoted as N_q on these figures.

Parameter	Value
μz_1	0.1
$\frac{z_2}{\mu^2}$	0.1
$\frac{X_0}{\mu^2}$	0.5
$\frac{k_0}{L\mu^2}$	0.1

Table 2: Parameters of the system.

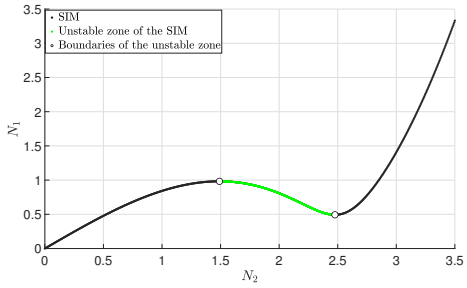

Figure 4: The SIM of the 1st mode of the continuous system for provided given from Table 2: stable and unstable zones of the SIM are depicted in black and green, respectively. The boundaries of stability are represented by white dots.

It is observed that as the mode number increases, the local minimum of the SIM becomes very close to the horizontal axis. This is in agreement with previously developed works [38, 47]: as the mode number increases, i.e. when μ increases, the equivalent damping of the non-dimensionalized equation, i.e. $\frac{z_2}{\mu}$ becomes smaller. When $\mu \to \infty$, it becomes zero, and the SIM touches the horizontal axis.

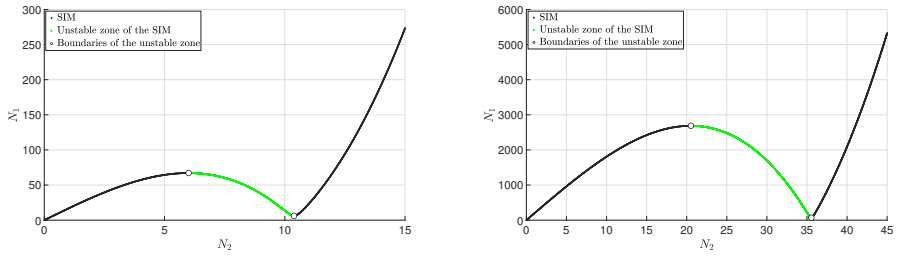

(a) (b)

Figure 5: The SIM of the a) 3rd, b) 10th modes of the continuous system for given parameters from Table 2: stable and unstable zones of the SIM are depicted in black and green, respectively. The boundaries of stability are represented by white dots.

3.2.2. Slow dynamics

The reduced system is studied at the order ε^1 to determine the equilibrium and singular points. As explained in Sect. 2.4.3, the equilibrium points are defined for $\mathscr{E} = 0$ (see Eq. (29)) with:

$$\mathscr{E} = \left[i\left(\sigma\left(1 + \frac{P_0}{L\mu^2}\right) - \frac{X_0}{\mu^2}\right) + \mu z_1 \right] \varphi_1 + i\frac{F_0}{\alpha\mu^2} + i\frac{X_0}{\mu^2}\varphi_2 \tag{53}$$

So the equation of the equilibrium points is:

$$a_c X^3 + b_c X^2 + c_c X + d_c = 0 \tag{54}$$

with $X = N_2^2$, where the coefficients of Eq. (54) are defined in Appendix A. Figures 6 and 7 represent the equilibrium points of the reduce system for the first and the second mode of the continuous system in modal domain, respectively, with a external excitation as $\dfrac{F_0}{\alpha\mu^2} = 1.1$ and for the parameters from Table 2. The equilibrium points located in the unstable zone of the SIM are represented in green. We can see that for the continuous system in the modal domain projected on the first mode, there are two branches: a main branch (i) and an isola (ii). Moreover, we can see that some equilibrium points are located in the unstable zone of the SIM of the first mode, while for the second mode (see Fig. 7) there is only one branch and the equilibrium points are all situated on the stable zone of the SIM. For numerical results we will focus on the first mode because it presents more interesting behavior.

Equation 54 provides equilibrium points of the reduced system enabling the prediction of the behavior of the system. We aim to compare the reduced system with the discrete one. To achieve this, the equilibrium points are plotted in the physical domain using Eq. (36). They depend on σ, N_{1CMPh} and N_{2CMPh} (see Fig. 8). For simplicity, N_{qCM} and N_{qCMPh} are denoted N_q $(q = 1, 2)$ on the figure axis.

According to Eq. (30) the singular points of the system are defined for $\det(\mathbb{B}) = 0$. From Eqs. (28) and (47), the matrix $\mathbb{B}$ is defined as [38]:

$$\mathbb{B} = \begin{bmatrix} \frac{z_2}{\mu} + i\left(1 - \frac{X_0}{\mu^2} - \frac{9P_0}{4L\mu^2}N_2^2\right) & -i\frac{9P_0}{8L\mu^2}\varphi_2^2 \\ i\frac{9P_0}{8L\mu^2}\varphi_2^{2*} & \frac{z_2}{\mu} - i\left(1 - \frac{X_0}{\mu^2} - \frac{9P_0}{4L\mu^2}N_2^2\right) \end{bmatrix} \tag{55}$$

So, the equation of the singular points ($\det(\mathbb{B}) = 0$) reads:

$$\frac{243}{64L^2\mu^4}P_0^2N_2^4 - \frac{9}{2}(1 - \frac{X_0}{\mu^2})\frac{P_0}{L\mu^2}N_2^2 + \frac{z_2^2}{\mu^2} + (1 - \frac{X_0}{\mu^2})^2 = 0 \tag{56}$$

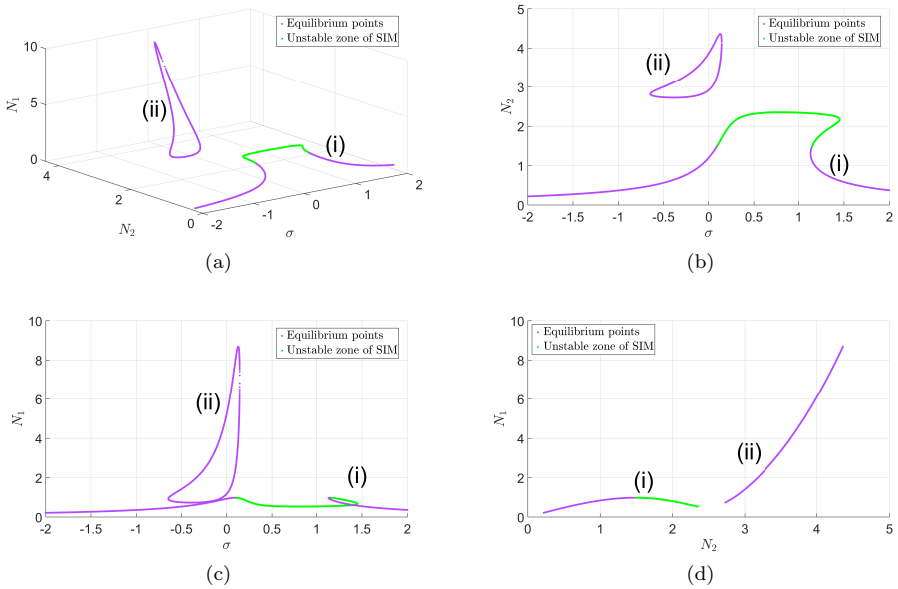

Figure 6: Equilibrium points for the first mode of the reduced system under external excitation as $\frac{F_0}{\alpha\mu^2} = 1.1$ a) Three-dimensioned view $(\sigma, N_{2CM}, N_{1CM})$; b) Two-dimensioned view (σ, N_{2CM}); c) Two dimensioned view (σ, N_{1CM}); d) Two-dimensioned view (N_{2CM}, N_{1CM}). Parameters of the system are reported in Table 2. Equilibrium points situated in unstable zone of the SIM are illustrated by green color.

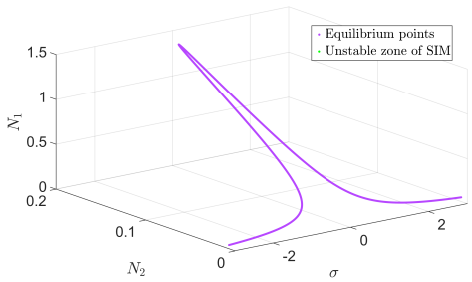

Figure 7: Equilibrium points for the second mode of the reduced system under external excitation as $\frac{F_0}{\alpha\mu^2} = 1.1$. Parameters of the system are reported in Table 2.

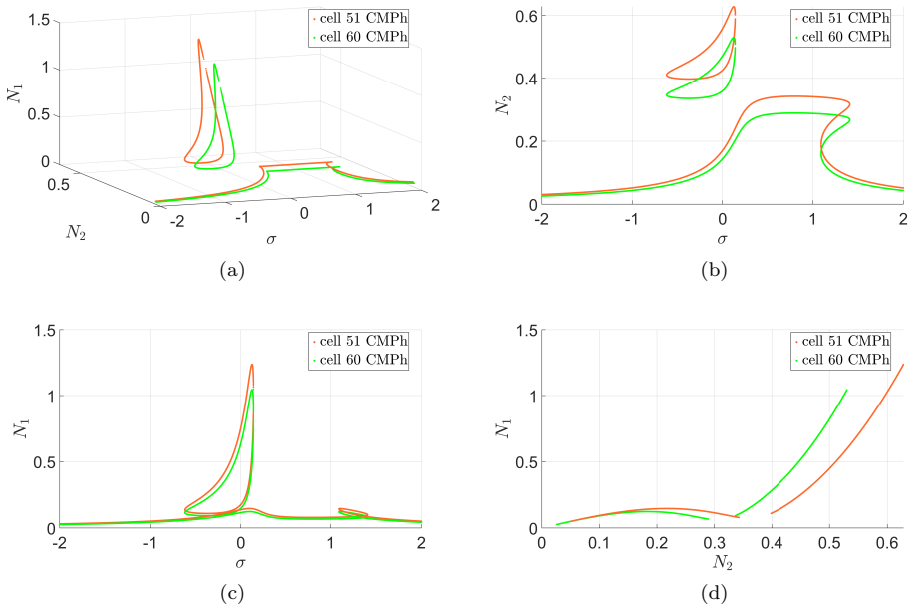

Figure 8: Equilibrium points in physical coordinates corresponding to cells 51 and 60 of the discrete chain ($x = j - 1$ where j stands for the cell number) under external excitation as $\frac{F_0}{\alpha\mu^2} = 1.1$ a) Three-dimensional view $(\sigma, N_{2CMPh}, N_{1CMPh})$; b) Two-dimensional view (σ, N_{2CMPh}); c) Two-dimensional view (σ, N_{1CMPh}); d) Two-dimensional view (N_{2CMPh}, N_{1CMPh}). Parameters of the system are reported in Table 2. Equilibrium points situated in unstable zone of the SIM are illustrated by green color.

We can find solutions of this equation which correspond to amplitudes of singular points. It is observed that Eq. (56) is identical to the equation that defines the boundaries of the unstable zone (see Eq. (52)). Consequently, it is observe that the singular points are located on the boundaries of the unstable zone. Thus, the equilibrium points in the unstable region of the SIM are unstable and correspond to a specific dynamical regime in a forced case. Indeed, the system is in a quasi-periodic regime; it does not converge to an equilibrium point but instead presents repeated bifurcations between the stable branches of the SIM.
In summary, through the analytical developments of this section, predictions have been made for the fast and slow dynamics of the continuous system in the modal domain: the SIM and its unstable zone for the fast dynamics, and the equilibrium and singular points for the slow dynamics.
In the next subsection, preliminary treatments are performed on the discrete chain to compare the obtained results with those of the reduced system from continuous equations in the modal domain.

3.3. Non-dimensionalized form of discrete equation of the chain

Since we consider the nonlinear restoring forcing function $\Lambda(v) = k_2 v_j^3(t)$, the non-dimensionalized equations of the discrete chain (see Eq. (32)) become:

$$\begin{cases} \dfrac{d^2u_j}{d\tau^2} + \dfrac{1}{\mu^2}(2u_j - u_{j+1} - u_{j-1}) + \dfrac{\varepsilon z_1}{\mu}\left(2\dfrac{du_j}{d\tau} - \dfrac{du_{j+1}}{d\tau} - \dfrac{du_{j-1}}{d\tau}\right) + \\ \qquad \dfrac{\varepsilon X_0}{\mu^2}(u_j - v_j) = \dfrac{\varepsilon F_0}{\mu^2}\cos(\mu(j-1))\sin(\nu\tau) \\ \\ \varepsilon\dfrac{d^2v_j}{d\tau^2} + \dfrac{\varepsilon P_0}{\mu^2}v_j^3 + \dfrac{\varepsilon z_2}{\mu}\dfrac{dv_j}{d\tau} + \dfrac{\varepsilon X_0}{\mu^2}(v_j - u_j) = 0 \end{cases} \tag{57}$$

In the next section, we will numerically integrate the governing equations of the continuous system in the modal coordinates and those of the discrete system to validate these predictions.

3.4. Numerical results

Parameter	Value
μz_1	0.1
$\dfrac{z_2}{\mu^2}$	0.1
$\dfrac{X_0}{\mu^2}$	0.5
$\dfrac{k_0}{L\mu^2}$	0.1
ε	0.01
L	100

Table 3: Parameters of the reduced system with a constant nonlinearity.

To validate the analytical predictions, numerical integrations (NI) are performed on Eq. (45) (reduced system) and Eq. (57) (discrete chain) with the Runge-Kutta method. As a representative example, we consider an excitation with a frequency around the first mode of the system. Four cases are considered. The first one corresponds to a free system with the parameters from Table 3 setting the external force $F_0 = 0$. The other three cases correspond to forced system with the parameters from Table 3 and $\dfrac{F_0}{\alpha\mu^2} = 1.1$ for different values of σ. The second case considers $\sigma = 0.5$. For this value, a single equilibrium point is located in the unstable zone of the SIM. The third and fourth cases consider $\sigma = -0.55$. For $\sigma = -0.55$, the reduced system has several possible equilibrium points, as shown in Fig. 6. Specifically, two of them are on the branch (ii), i.e. the isola, and one of them is on the main

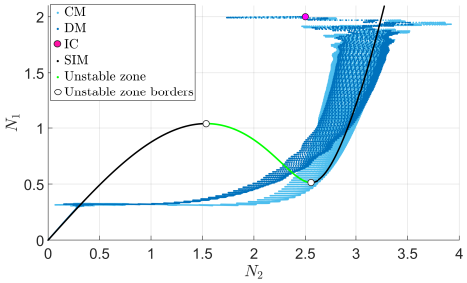

Figure 9: NI of Eq. (45) in light blue (reduced system) and Eq. (57) in dark blue (discrete chain in modal domain), SIM of the reduced system (in black), its unstable zone (in green), the boundaries of the unstable zone (white dots) and the ICs (pink dot) for parameters from Table 3, $F_0 = 0$, $(g(\tau = 0), h(\tau = 0), \dot{g}(\tau = 0), \dot{h}(\tau = 0)) = (2, 2.5, 0, 0)$.

branch (i). Two NI with different initial conditions (ICs) are performed to reach the isola and the main branch. The ICs of the discrete chain are set as $u_j(\tau = 0) = \alpha \cos(\mu \times (j-1))g(\tau = 0)$ and $v_j(\tau = 0) = \alpha \cos(\mu \times (j-1))h(\tau = 0)$ where $g(\tau = 0)$ and $h(\tau = 0)$ are the ICs of the reduced system and $j = 1, ...L$. Furthermore, to present the results in the physical domain, obtained from the discrete chain and the reduced system, the focus will be on only two cells: the 51^{st} and the 60^{th} cells. This choice is made because these two cells are located at antinode levels and exhibit large displacements compared to cells at node levels, where different regimes may be more difficult to observe. Further details on this choice are discussed in Sect. 3.4.2. On the axis of the figures, N_{qCM}, N_{qCMPh}, N_{qDM} and N_{qDPh} are denoted as N_q $(q = 1, 2)$.

3.4.1. Case I: free system

First, we consider a free system, i.e. $F_0 = 0$ and the following ICs $(g(\tau = 0), h(\tau = 0), \dot{g}(\tau = 0), \dot{h}(\tau = 0)) = (2, 2.5, 0, 0)$. Figure 9 illustrates the NI of Eq. (45) in light blue (representing the reduced system) and that of Eq. (57) in dark blue (representing the discrete system in the modal domain). The ICs are represented by a pink dot, the SIM is represented by a dark line, the unstable zone of the SIM is represented by a green line and the boundaries of the unstable zone/singular points are marked by white dots. Figures 10a, 10b illustrate the time responses N_{qDM} and N_{qCM} as functions of τ, respectively. The time responses of cells 51 and 60 for N_{qCMPh} and N_{qDPh} are presented in Figs. 11a and 11b $(q = 1, 2)$.

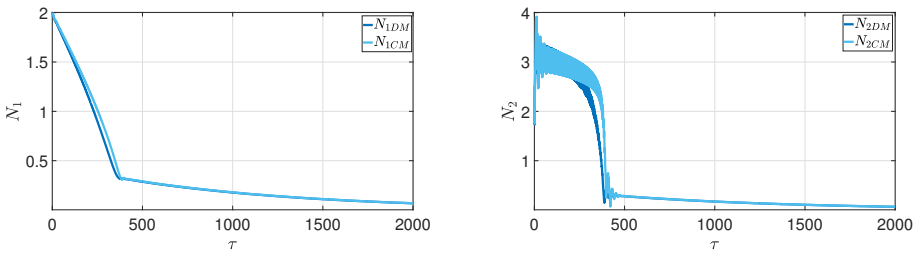

(a) (b)

Figure 10: a) N_{1DM} and N_{1CM} as functions of τ; b) N_{2DM} and N_{2CM} as functions of τ (dark blue and light blue, respectively); for parameters from Table 3, $F_0 = 0$, $(g(\tau = 0), h(\tau = 0), \dot{g}(\tau = 0), \dot{h}(\tau = 0)) = (2, 2.5, 0, 0)$.

Figure 9 shows that the NI of the reduced system (depicted in light blue) follows the upper stable

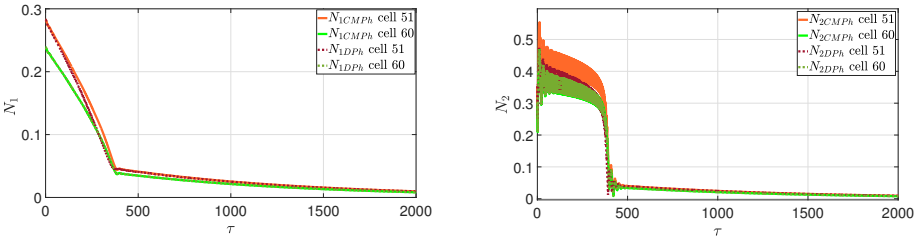

(a) (b)

Figure 11: a) N_{1DPh} and N_{1CMPh} as functions of τ; b) N_{2DPh} and N_{2CMPh} as functions of τ of cells 51 and 60 (dark red, dark green, orange and light green, respectively); for parameters from Table 3, $F_0 = 0$, $(g(\tau = 0), h(\tau = 0), \dot{g}(\tau = 0), \dot{h}(\tau = 0)) = (2, 2.5, 0, 0)$. For the continuous system $x = j - 1$ where j stands for the cell number.

branch on the SIM until the unstable zone. Then, it jumps to the other stable branch of the SIM and finally, the system converges to zero as excepted. The NI of the discrete system in the modal domain (presented in dark blue) presents the same behavior as the reduced system, although the jump is less precise. This discrepancy may result from different factors such as keeping only the first harmonic in the analytical developments, approximating the overall behavior of the chain by a single mode and neglecting internal resonances and the effect of the ε parameter. This shift is also present in the time responses in Figs. 10 and 11. The N_1 responses of the different systems are very close. However, for N_2 we can observe that the jump does not occur exactly at the same time for the 2 dof systems and the cell 51 does not reach the same amplitude for the continuous system in the physical domain and discrete chain. In summary, despite the approximation of the response of the overall chain by considering only one of its modes, the analytical developments based on this assumption are in good qualitative agreement with those obtained by projecting of the chain on only one of its modes.

3.4.2. Forced system

In order to have a better understanding of the attraction of the system to different possible regimes, basins of attractions are plotted for the first cell of the discrete chain (see Figs. 12a and 12b) and for the reduced system (see Figs. 12c and 12d) using the parameters from Table 3 and $\dfrac{F_0}{\alpha\mu^2} = 1.1$. These plots are accompanied by the equilibrium points (violet line) and the unstable zone of the SIM (green line) (see Fig. 6). We can point out that the basin of attraction is the same for the cell 51 and for the cell 1, given that the chain is periodic and follows the first mode, with a force of the form $F_j = \alpha F \cos(\mu(j-1))$. The coordinates of the points on the basins of attractions correspond to ICs of the NI and the color represents the attracted regime of the system. In this case, we can discern the behavior of the system based on the ICs and the excitation frequency ($\nu = 1 + \sigma\varepsilon$). For the reduced system, we have (see Eq. (19)):

$$\begin{cases} N_{1CM}(\tau = 0) = |\dot{g}(\tau = 0) + i\nu g(\tau = 0)| \\ N_{2CM}(\tau = 0) = |\dot{h}(\tau = 0) + i\nu h(\tau = 0)| \end{cases} \tag{58}$$

Since we consider $\dot{g}(\tau = 0) = 0$ and $\dot{h}(\tau = 0) = 0$, we can express:

$$\begin{cases} N_{1CM}(\tau = 0) = |g(\tau = 0)| \\ N_{2CM}(\tau = 0) = |h(\tau = 0)| \end{cases} \tag{59}$$

For the discrete chain, we have (see Eq. (38)):

$$\begin{cases} N_{1DM,j}(\tau = 0) = |\dot{u}_j(\tau = 0) + i\nu u_j(\tau = 0)| \\ N_{2DM,j}(\tau = 0) = |\dot{v}_j(\tau = 0) + i\nu v_j(\tau = 0)| \end{cases} \tag{60}$$

So,

$$\begin{cases} N_{1DM,j}(\tau=0) = |\dot{u}_j(\tau=0)| = \alpha\cos(\mu\times(j-1))g(\tau=0) \\ N_{2DM,j}(\tau=0) = |\dot{v}_j(\tau=0)| = \alpha\cos(\mu\times(j-1))h(\tau=0) \end{cases} \tag{61}$$

The axis N_1 and N_2 correspond to the ICs $g(\tau=0)$ and $h(\tau=0)$. In Fig. 12, the red, light blue and dark blue dots correspond to a system that reaches a quasi-periodic regime, the isolated or the main branch of the frequency responses (see Fig. 6) (periodic regimes), respectively. For both systems, a similar organization is observed, which is clearer for $N_1(\tau=0)$ and σ than for $N_2(\tau=0)$ and σ. For $\sigma > 0.1$, both systems are in the quasi-periodic regime, as predicted by the unstable zone of the SIM. As shown in [47], the existence of singularities can lead the system to exhibit a quasi-periodic response. Moreover, if the system has only one equilibrium point located in the unstable zone of the SIM, then the system will present quasi-periodic regime [48]. For the first cell of the discrete chain for $\sigma \in [-0.4; 0.1]$, $N_1(\tau=0) \in [0; 8]$ and $N_2(\tau=0) \in [0; 5]$, it is noticeable that the cell is on the isola regardless of the IC. For the reduced system, a similar behavior is observed for $\sigma \in [-0.3; 0.1]$. For smaller values of σ, several groups (isola or main branch) are observed which depend more on $N_1(\tau=0)$, i.e. $g(\tau=0)$, and σ than on $N_2(\tau=0)$,i.e. $h(\tau=0)$, (see Figs. 12c and 12a). In summary, the behavior depends more on $N_1(\tau=0)$ and σ than on $N_2(\tau=0)$. It is important to note that for the discrete chain, only the first cell (and so the 51^{st} cell) is considered, which may not be fully representative of the general behavior of the entire chain. In the rest of this subsection, some

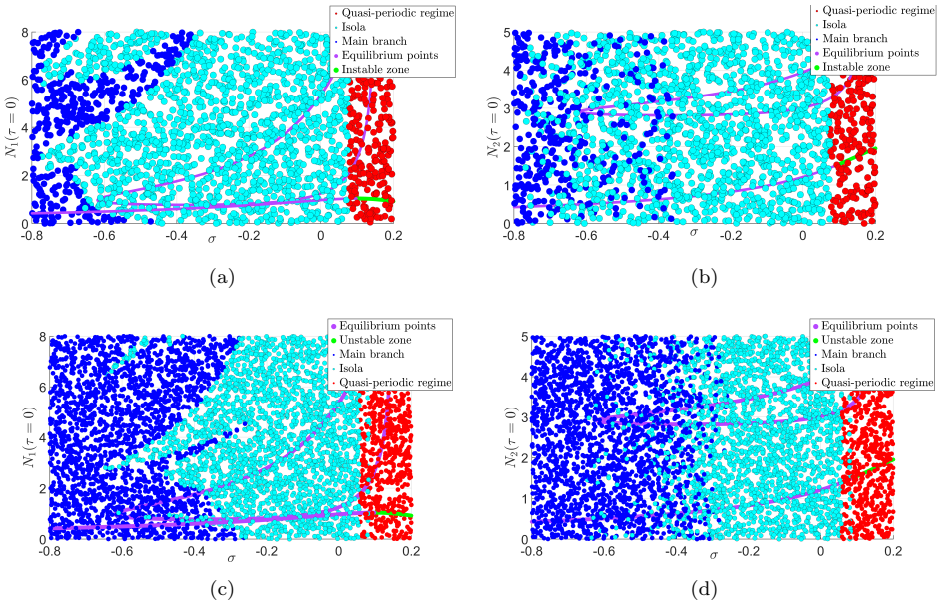

Figure 12: Basins of attractions a) $N_{1DPh,1}$ as a function of σ; b) $N_{2DPh,1}$ as a function of σ; c) N_{1CM} as a function of σ; d) N_{2CM} as a function of σ.

results will be presented for the forced systems with $\dfrac{F_0}{\alpha\mu^2} = 1.1$ but with different values of detuning parameters, σ, and IC.

Case II: $\sigma = 0.5$, $\dfrac{F_0}{\alpha\mu^2} = 1.1$, $(g(\tau=0), h(\tau=0)) = (0,0)$

In this part, forced systems are examined and the analytical developments are compared with the numerical results for the parameters from Table 3, with $\sigma = 0.5$ and the ICs given by $(g(\tau = 0), h(\tau = 0), \dot{g}(\tau = 0), \dot{h}(\tau = 0)) = (0, 0, 0, 0)$. Figure 13 illustrates the SIM of the first mode of the reduced system (represented by the black line) accompanied by the numerical results of the reduced system (light blue line) and the discrete chain in the modal domain (dark blue line). The time responses of N_{qCM} and N_{qDM} are presented in Fig. 14 and those of N_{qDPh} and N_{qCMPh} (for cells 51 and 60) are presented in Fig. 15. To provide a clearer understanding of the behavior of the systems, three-dimensional views of the time responses of $N_{qDPh,j}(\tau)$ and $N_{qCMPh}(x, \tau)$ as functions of mass number (j) and space (x) are depicted in Fig. 16 $(q = 1, 2)$.
In Fig. 13, the response of the reduced system obtained from NI exhibits repeated bifurcations between stable branches of the SIM. This corresponds to the predictions shown in Fig. 6: the only equilibrium point for this value of σ is located in the unstable zone of the SIM. The NI of the discrete system in the modal basis presents the same behavior but with less precision, especially for N_2. Indeed, all predictions based on the reduced form of the continuous system show an averaged behavior of the entire chain around one of its modes, while results obtained from the direct NI of the overall chain cover whole system behavior. In Fig. 16, we observe that the discrete and continuous systems in the physical domain follow the form of the absolute value of the first linear mode of the continuous system, i.e. $\alpha \cos(\mu x)$. Thus some cells are situated near nodes (cells 26 and 76), which do not move much, while others are near an antinode (cells 1 and 51) which have large displacements. For this reason, cell 51 and cell 60 are chosen to study of the discrete chain. Cell 60 is slightly offset from the antinode but remains close. If we compare Figs. 16a, 16b and 16c, we can see that N_{1CMPh}, N_{2CMPh} and N_{1DPh} closely follow the shape of the mode while for N_{2DPh} in Fig. 16d the response deviates somewhat from the linear mode.

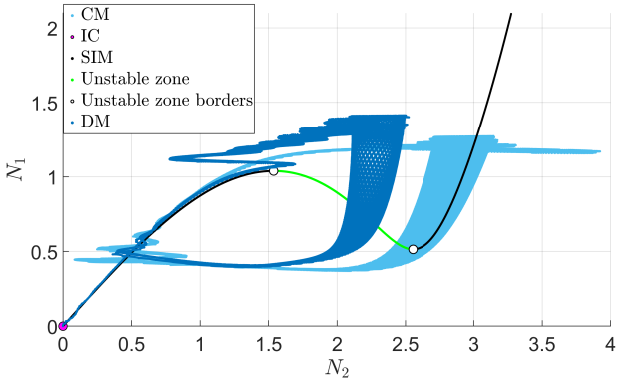

Figure 13: NI of Eq. (45) in light blue (reduced system) and Eq. (57) in dark blue (discrete chain in modal domain), SIM of the reduced system (in black), its unstable zone (in green), the boundaries of the unstable zone (white dots) and the ICs (pink dot) for parameters from Table 3, $\dfrac{F_0}{\alpha\mu^2} = 1.1$, $\sigma = 0.5$, $(g(\tau = 0), h(\tau = 0), \dot{g}(\tau = 0), \dot{h}(\tau = 0)) = (0, 0, 0, 0)$.

To better understand the quasi-periodic behavior, the Poincaré map [49] is plotted for the 2 dof systems (the reduced system and the discrete system in the modal domain). For a system in quasi-periodic, the Poincaré map corresponds to a closed loop, while for a system in a periodic regime, it ideally corresponds to a point. The discrete and continuous systems in the modal domain are plotted in Figs. 17a and 17b ($\dot{g}_D(\tau)$ as a function of $g_D(\tau)$, $\dot{g}(\tau)$ as a function of $g(\tau)$, $\dot{h}_D(\tau)$ as a function of $h_D(\tau)$ and $\dot{h}(\tau)$ as a function of $h(\tau)$, respectively). The Poincaré maps of the 2L dof systems are not plotted to avoid overloading the paper; indeed Figs. 14 and 15 already highlight the differences between the systems. It is noteworthy that the global geometry of Poincaré maps looks like a closed loop which corresponds well to a quasi-periodic regime.

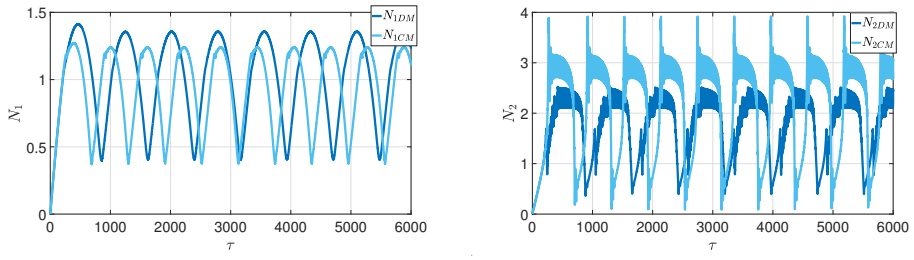

(a) (b)

Figure 14: a) N_{1DM} and N_{1CM} as functions of τ; b) N_{2DM} and N_{2CM} as functions of τ (dark blue and light blue, respectively); for parameters from Table 3, $\frac{F_0}{\alpha\mu^2} = 1.1$, $\sigma = 0.5$, $(g(\tau=0), h(\tau=0), \dot{g}(\tau=0), \dot{h}(\tau=0)) = (0,0,0,0)$.

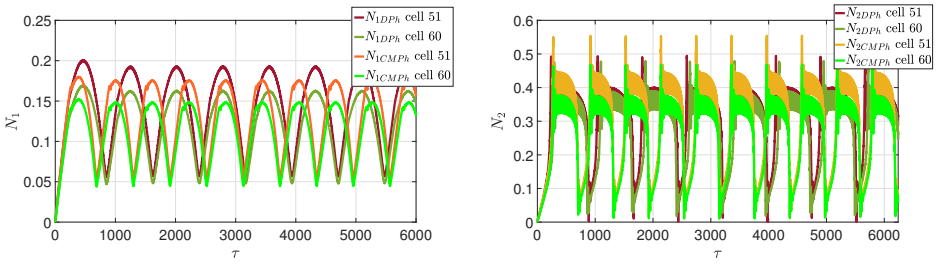

(a) (b)

Figure 15: a) N_{1DPh} and N_{1CMPh} as functions of τ; b) N_{2DPh} and N_{2CMPh} as functions of τ of cells 51 and 60 (dark red, dark green, orange and light green, respectively); for parameters from Table 3, $\frac{F_0}{\alpha\mu^2} = 1.1$, $\sigma = 0.5$, $(g(\tau=0), h(\tau=0), \dot{g}(\tau=0), \dot{h}(\tau=0)) = (0,0,0,0)$. For the continuous system $x = j-1$ where j stands for the cell number.

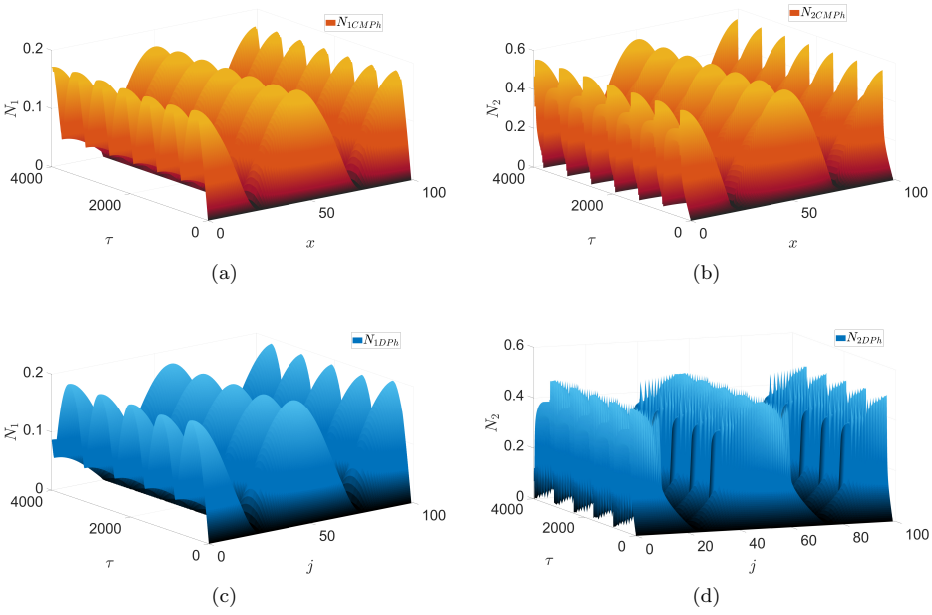

Figure 16: Three-dimensional view of a) $N_{1CMPh}(x,\tau)$; b) $N_{2CMPh}(x,\tau)$; c) $N_{1DPh,j}(\tau)$; d) $N_{2DPh,j}(\tau)$; for parameters from Table 3, $\dfrac{F_0}{\alpha\mu^2} = 1.1$, $\sigma = 0.5$, $(g(\tau=0), h(\tau=0), \dot{g}(\tau=0), \dot{h}(\tau=0)) = (0,0,0,0)$.

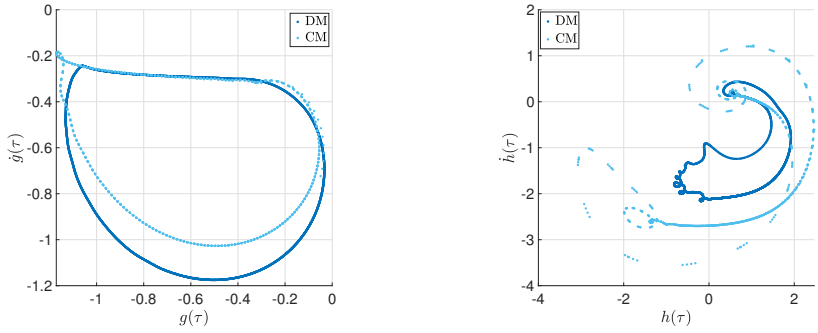

Figure 17: Poincaré maps a) $\dot{g}_D(\tau)$ as a function of $g_D(\tau)$ and $\dot{g}(\tau)$ as a function of $g(\tau)$, b) $\dot{h}_D(\tau)$ as a function of $h_D(\tau)$ $\dot{h}(\tau)$ as a function of $h(\tau)$ (dark blue and light blue); for parameters from Table 3, $\dfrac{F_0}{\alpha\mu^2} = 1.1$, $\sigma = 0.5$, $(g(\tau=0), h(\tau=0), \dot{g}(\tau=0), \dot{h}(\tau=0)) = (0,0,0,0)$.

To observe the effects of different harmonics on the system responses, we filter the results obtained from the direct NI keeping only the first and the third harmonics for the reduced and discrete systems in the modal domain. Figures 18 and 19 summarize results for N_{qDM} and N_{qCM} $(q = 1, 2)$, for the

filtered first and third harmonics, respectively. For N_1, the first harmonic provides a good representation of the overall response while the third harmonic has an almost negligible effect on overall response (see Fig. 18b). On the contrary, for N_2, the first harmonic corresponds to the average amplitude and the third harmonic has a more significant effect on values of N_2 compared to the first harmonic (see Fig. 19b), it takes into account the oscillations. This can explain the difference between the N_2 values obtained directly from the reduced form of continuous system and those obtained from the discrete chain as depicted in Fig. 13. In fact, for detecting the SIM, only the first harmonics of the system are kept, see Eq. (22), while filtering the data shows that the third harmonic of the N_2 plays an important role in the system responses. However, the analytical developments based on keeping only the first harmonic are able to qualitatively predict system responses during extreme nonlinear interactions in the system.

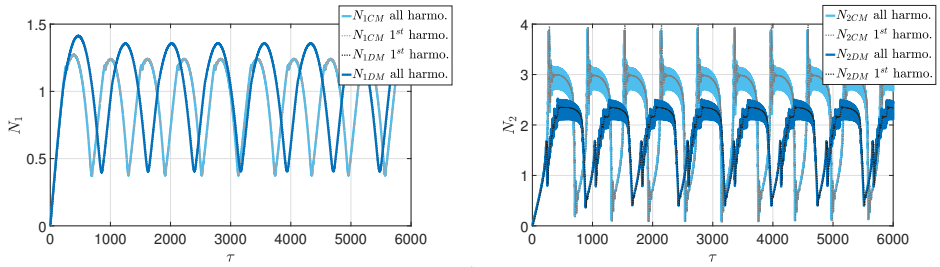

(a) (b)

Figure 18: Filtering around the first harmonic and the response with all the harmonics a) N_{1DM} and N_{1CM} as functions of τ; b) N_{2DM} and N_{2CM} as functions of τ of the discrete chain in the modal domain (black dotted line, dark blue line, gray dotted line and light blue line, respectively); for parameters from Table 3, $\frac{F_0}{\alpha\mu^2} = 1.1$, $\sigma = 0.5$, $(g(\tau=0), h(\tau=0), \dot{g}(\tau=0), \dot{h}(\tau=0)) = (0,0,0,0)$.

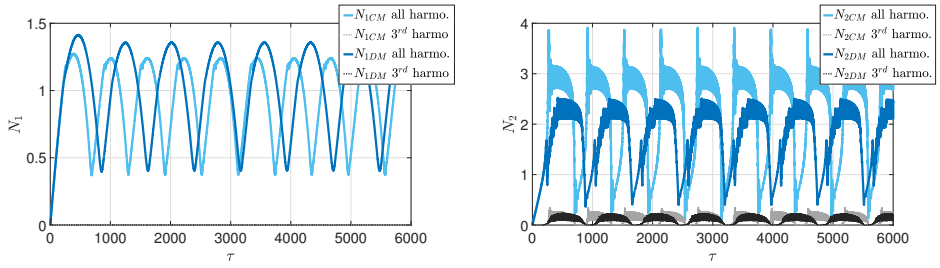

(a) (b)

Figure 19: Filtering around the first harmonic and the response with all the harmonics a) N_{1DM} and N_{1CM} as functions of τ; b) N_{2DM} and N_{2CM} as functions of τ (black dotted line, dark blue line, gray dotted line and light blue line, respectively); for parameters from Table 3, $\frac{F_0}{\alpha\mu^2} = 1.1$, $\sigma = 0.5$, $(g(\tau=0), h(\tau=0), \dot{g}(\tau=0), \dot{h}(\tau=0)) = (0,0,0,0)$.

Case III: $\sigma = -0.55$**,** $\frac{F_0}{\alpha\mu^2} = 1.1$**,** $(g(\tau=0), h(\tau=0)) = (0,0)$

For the third case, we consider the parameters from Table 3, with $\sigma = -0.55$ and the following ICs $(g(\tau=0), h(\tau=0), \dot{g}(\tau=0), \dot{h}(\tau=0)) = (0,0,0,0)$. According to Fig. 6, for $\sigma = -0.55$,

there are three possible equilibrium points situated on the main branch and also on the isola. The basin of attractions (see Fig. 12) shows that for mentioned IC, both discrete and reduced systems should be attracted by the main branch. Figure 20 illustrates the SIM of the first mode of the reduced system accompanied by numerical results of the continuous (light blue line) and discrete (dark blue line) systems in the modal domain. The time responses of N_{qCM} and N_{qDM} of cells 51 and 60 are presented in Fig. 21, N_{qDPh} and N_{qCMPh} are illustrated in Fig. 22 ($q = 1, 2$). Figures 23a and 23b show N_{qCMPh} as a function of x and τ and Figs. 23c and 23d represent N_{qDPh} as a function of j and τ ($q = 1, 2$).

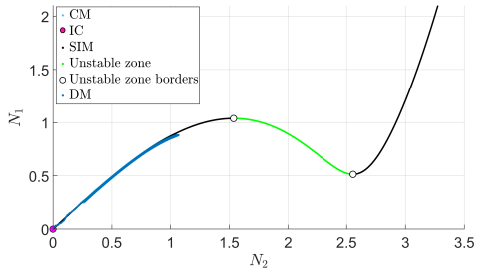

Figure 20: NI of Eq. (45) in light blue (reduced system) and Eq. (57) in dark blue (discrete chain in modal domain), SIM of the reduced system (in black), its unstable zone (in green), the boundaries of the unstable zone (white dots) and the ICs (pink dot) for parameters from Table 3, $\frac{F_0}{\alpha\mu^2} = 1.1$, $\sigma = -0.55$, $(g(\tau = 0), h(\tau = 0), \dot{g}(\tau = 0), \dot{h}(\tau = 0)) = (0, 0, 0, 0)$.

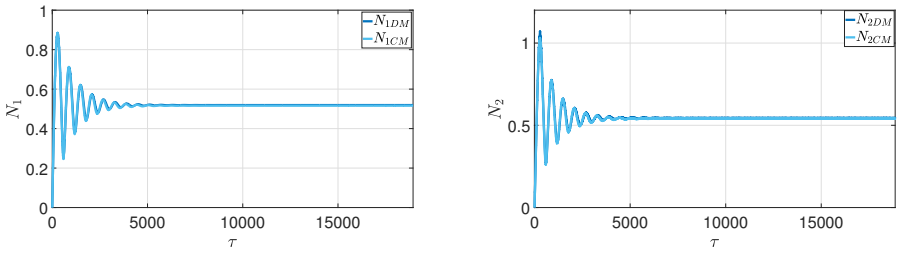

(a) (b)

Figure 21: a) N_{1DM} and N_{1CM} as functions of τ; b) N_{2DM} and N_{2CM} as functions of τ (dark blue and light blue, respectively); for parameters from Table 3, $\frac{F_0}{\alpha\mu^2} = 1.1$, $\sigma = -0.55$, $(g(\tau = 0), h(\tau = 0), \dot{g}(\tau = 0), \dot{h}(\tau = 0)) = (0, 0, 0, 0)$.

In Fig. 20, we observe that both systems follow the SIM and reach an equilibrium point on the lower branch. Futhermore, Figs. 21 and 22 show that the response of both systems are very similar and that the reduced system accurately describes the behavior of the discrete one. The responses of all cells in the discrete chain are almost identical to those of the reduced form of the continuous system (see Fig. 23). Unlike case II, where there are some differences between different values of N_2 (from different systems), here the attracted equilibrium point is on the lower branch of the SIM (see Fig. 21). Therefore, the nonlinearity of the system is less activated compared to the case II, leading to weaker effects of higher harmonics and internal resonances. All this contributes to good predictions of the system behavior after projection on a single mode. Thus, the analytical predictions are validated as the reduced system and the discrete system in the modal domain converge to $N_{1CM} = 0.52$ and $N_{2CM} = 0.54$ as predicted in Fig. 6.

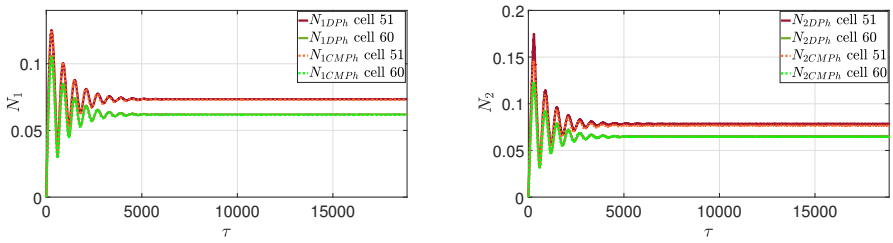

(a) (b)

Figure 22: a) N_{1DPh} and N_{1CMPh} as functions of τ; b) N_{2DPh} and N_{2CMPh} as functions of τ of cells 51 and 60 (dark red, dark green, orange and light green, respectively); for parameters from Table 3, $\frac{F_0}{\alpha\mu^2} = 1.1$, $\sigma = -0.55$, $(g(\tau=0), h(\tau=0), \dot{g}(\tau=0), \dot{h}(\tau=0)) = (0,0,0,0)$.

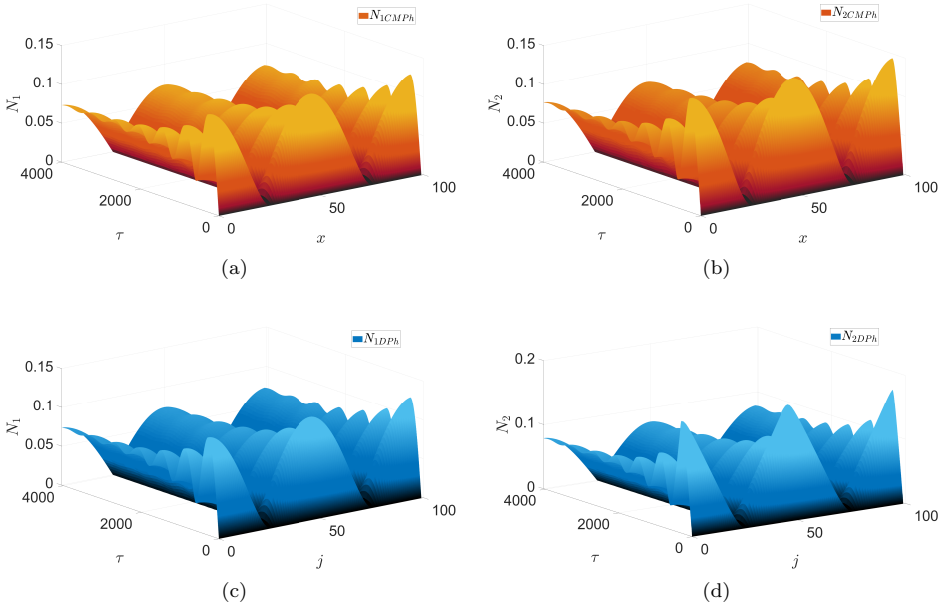

(a) (b)

(c) (d)

Figure 23: Three-dimensional view of a) $N_{1CMPh}(x,\tau)$; b) $N_{2CMPh}(x,\tau)$; c) $N_{1DPh,j}(\tau)$; d) $N_{2DPh,j}(\tau)$; for parameters from Table 3, $\frac{F_0}{\alpha\mu^2} = 1.1$, $\sigma = -0.55$, $(g(\tau=0), h(\tau=0), \dot{g}(\tau=0), \dot{h}(\tau=0)) = (0,0,0,0)$. For the continuous system $x = j-1$ where j stands for the cell number.

Case IV: $\sigma = -0.55$, $\dfrac{F_0}{\alpha\mu^2} = 1.1$, $(u_1(\tau=0), u_2(\tau=0)) = (3.3, 0)$

Let us consider the parameters from Table 3 with $\sigma = -0.55$ and the following ICs $(g(\tau=0), h(\tau=0), \dot{g}(\tau=0), \dot{h}(\tau=0)) = (3.3, 0, 0, 0)$. Figure 24 represents the SIM of the first mode of the reduced system with numerical results of the continuous and discrete systems in the modal domain. Figure 25 corresponds to the time histories of N_{qCM} and N_{qDM} and Fig. 26 represents N_{qCMPh} and N_{qDPh} of cells 51 and 60 ($q = 1, 2$). The ICs are higher than for case III. The systems converge to an equilibrium point on the isola corresponding to a high energy level of the main system (see Figs. 25 and 26). N_{1CM} and N_{1DM} (see Fig. 25a) as well as N_{2CM} and N_{2DM} (see Fig. 25b) are close but do not converge to exactly the same points. Indeed for the discrete chain, the cells close to a node, do not have enough energy the reach the isola, creating a shift compared to the reduced system. We can also notice that for the discrete chain, N_{2DPh} of cells 51 and 60 have almost the same amplitude in stationary regime (after $\tau = 500$) (see Fig. 26b).

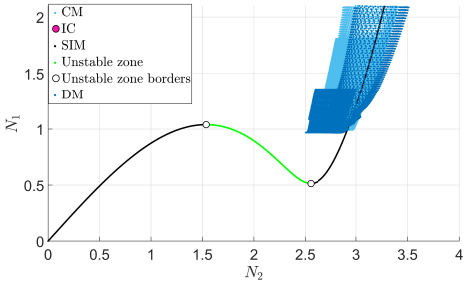

Figure 24: NI of Eq. (45) in light blue (reduced system) and Eq. (57) in dark blue (discrete chain in modal domain), SIM of the reduced system (in black), its unstable zone (in green), the boundaries of the unstable zone (white dots) and the ICs (pink dot) for parameters from Table 3, $\dfrac{F_0}{\alpha\mu^2} = 1.1$, $\sigma = -0.55$, $(g(\tau=0), h(\tau=0), \dot{g}(\tau=0), \dot{h}(\tau=0)) = (3.3, 0, 0, 0)$.

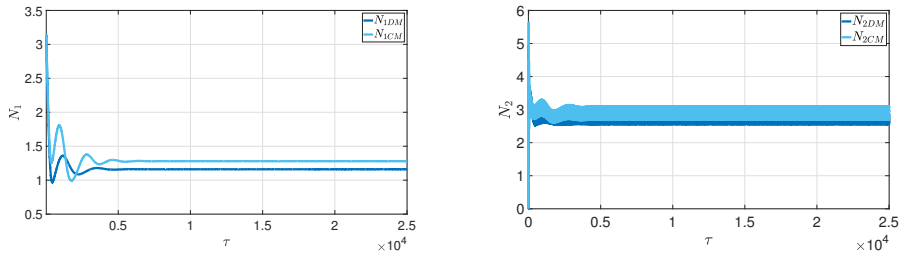

(a) (b)

Figure 25: a) N_{1DM} and N_{1CM} as functions of τ; b) N_{2DM} and N_{2CM} as functions of τ (dark blue and light blue, respectively); for parameters from Table 3, $\dfrac{F_0}{\alpha\mu^2} = 1.1$, $\sigma = -0.55$, $(g(\tau=0), h(\tau=0), \dot{g}(\tau=0), \dot{h}(\tau=0)) = (3.3, 0, 0, 0)$.

3.5. Conclusion

The reduced and discrete systems were considered for a constant stiffness and a cubic restoring force. An analytical study of the reduced system, including the detection of its fast and slow dynamics,

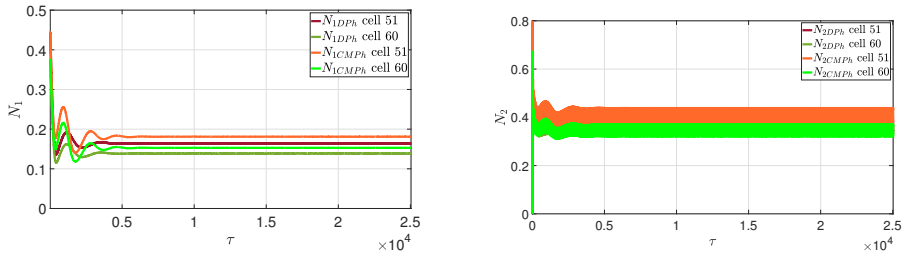

(a) (b)

Figure 26: a) N_{1DPh} and N_{1CMPh} as functions of τ; b) N_{2DPh} and N_{2CMPh} as functions of τ of cells 51 and 60 (dark red, dark green, orange and light green, respectively); for parameters from Table 3, $\dfrac{F_0}{\alpha\mu^2} = 1.1$, $\sigma = -0.55$, $(g(\tau=0), h(\tau=0), \dot{g}(\tau=0), \dot{h}(\tau=0)) = (3.3, 0, 0, 0)$. For the continuous system $x = j - 1$ where j stands for the cell number.

has led to the definition of the SIM, equilibrium and singular points. Numerical integrations of both systems for different cases on the one hand validate the analytical predictions and on the other hand show that the reduced system globally predicts the response of the discrete chain, although there are some discrepancies between the responses of selected cells.

4. Presentation of the system possessing a variable cubic nonlinear stiffness

In this section, a time-dependent nonlinearity will be considered. The method described in Sect. 2 will be used to study the different dynamics of the reduced system.

4.1. General presentation of the system

Let us assume that the nonlinear restoring forcing function $\Lambda(v)$ (see Eq. (1)) is cubic and time-dependent. It is defined as follows:

$$\Lambda(v) = k_2(t) v_j^3(t) \tag{62}$$

In the continuous domain $\Lambda(v)$ is given by:

$$\Lambda(v) = k_2(t) v^3 = k_2(t) A_k(x)^3 h_k(t)^3 \tag{63}$$

The non-dimensionalized equations of the continuous system in the modal domain (see Eq. (18)) reads:

$$\begin{cases} \dfrac{d^2 g}{d\tau^2} + g(\tau) + \varepsilon z_1 \mu \dfrac{dg}{d\tau} + \dfrac{\varepsilon X_0}{\mu^2}(g(\tau) - h(\tau)) = \dfrac{\varepsilon F_0}{\alpha\mu^2}\sin(\nu\tau) \\ \varepsilon \dfrac{d^2 h}{d\tau^2} + \dfrac{3\varepsilon P_0(\tau)}{2L\mu^2} h(t)^3 + \dfrac{\varepsilon z_2}{\mu}\dfrac{dh}{d\tau} - \dfrac{\varepsilon X_0}{\mu^2}(g(\tau) - h(\tau)) = 0 \end{cases} \tag{64}$$

with $\varepsilon P_0(\tau) = \frac{k_2(\tau)}{k_1}$. We assume that $P_0(\tau)$ is $\frac{2\pi}{\nu}$ periodic around a constant value K_0 and that it can be developed in terms of Fourier series, as follows:

$$P_0(\tau) = \sum_{n=-\infty}^{n=+\infty} K_n e^{in\nu\tau} \tag{65}$$

For the analytical development φ_{qCM}, N_{qCM} and δ_{qCM} will be denoted as φ_q, N_q and δ_q $(q = 1, 2)$. After introducing the complex variables of Manevitch [42] the Galerkin technique is applied, Eq. (22) reads:

$$\begin{cases} \dot{\varphi}_1 + \dfrac{i}{2}\nu\varphi_1 + \dfrac{1}{2}\varepsilon\mu z_1\varphi_1 + \dfrac{1}{2i\nu}\varphi_1 + \varepsilon\dfrac{X_0}{\mu^2}\dfrac{1}{2i\nu}(\varphi_1 - \varphi_2) = \dfrac{\varepsilon F_0}{2i\alpha\mu^2} \\ \varepsilon(\dot{\varphi}_2 + \dfrac{i}{2}\nu\varphi_2) + \dfrac{1}{2}\varepsilon\dfrac{z_2}{\mu}\varphi_2 + \varepsilon\dfrac{X_0}{\mu^2}\dfrac{1}{2i\nu}(\varphi_2 - \varphi_1) + \varepsilon G(u_2) = 0 \end{cases} \tag{66}$$

with

$$G(\varphi_2, \varphi_2^*) = \frac{i}{8\nu^3}\left[\varphi_2^3 K_{-2} - 3K_0|\varphi_2|^2\varphi_2 + 3K_2|\varphi_2|^2\varphi_2^* - \varphi_2^{*3}K_4\right] \tag{67}$$

As explained in Sect. 2.4, in the next subsection, different dynamics of the reduced system will be detected leading to the determination of characteristic points of the reduced system.

4.2. Detection of different dynamics of reduced system

4.2.1. Fast dynamics

For this subsection, Eq. (66) is considered at the ε^0 order. As in Sect 3.2.1, we seek $\mathscr{H}(\varphi_1, \varphi_2) = 0$ with

$$\mathscr{H} = \frac{1}{2}i\varphi_2 + \frac{z_2}{2\mu}\varphi_2 - \frac{iX_0}{2\mu^2}(\varphi_2 - \varphi_1) + \frac{i}{8}\left[\varphi_2^3 K_{-2} - 3K_0|\varphi_2|^2\varphi_2 + 3K_2|\varphi_2|^2\varphi_2^* - \varphi_2^{*3}K_4\right] \tag{68}$$

So, considering $K_0 \in \mathbb{R}$, $K_j = k_{jR} + ik_{jI}$, $j = \{2, 4\}$ and $K_{-j} = K_j^*$, the equation of the SIM in real domain (see Eq. (26)) reads:

$$N_1 = \frac{N_2\mu^2}{X_0}\sqrt{A^2 + B^2} \tag{69}$$

$$\delta_1 = \delta_2 + \arctan\left(\frac{B}{A}\right) \tag{70}$$

where $A(N_2, \delta_2)$ and $B(N_2, \delta_2)$ are defined in Appendix B. Thus, the SIM of the reduced system depends on the phase δ_2 in addition to N_1 and N_2. To determine the boundaries of the unstable zones of the SIM, we are interested in the second equation of Eq. (66) which is written:

$$\frac{\partial\varphi_2}{\partial\tau_0} + \frac{1}{2}\left[i\varphi_2 + \frac{z_2}{\mu}\varphi_2 - i\frac{X_0}{\mu^2}(\varphi_2 - \varphi_1) + \frac{i}{4}\left(\varphi_2^3 K_2^* - 3\varphi_2^2\varphi_2^* K_0 + 3\varphi_2\varphi_2^{*2}K_2 - \varphi_2^{*3}K_4\right)\right] = 0 \tag{71}$$

After considering the complex conjugate of Eq. (71), and introducing a perturbation on φ_2 ($\varphi_2 \to \varphi_2 + \Delta\varphi_2$) and its complex conjugate φ_2^* ($\varphi_2^* \to \varphi_2^* + \Delta\varphi_2^*$), we obtain:

$$\begin{pmatrix} \dfrac{\partial\Delta\varphi_2}{\partial\tau_0} \\ \dfrac{\partial\Delta\varphi_2^*}{\partial\tau_0} \end{pmatrix} = \mathbb{M}_v \begin{pmatrix} \Delta\varphi_2 \\ \Delta\varphi_2^* \end{pmatrix} \tag{72}$$

where $\mathbb{M}_v$ is detailed in Appendix C. Using the method described in Sect. 3.2.1 the boundaries of the unstable zone of the SIM correspond to:

$$a_v N_2^4 + b_v N_2^2 + c_v = 0 \tag{73}$$

with a_v, b_v and c_v defined in Appendix D.

4.2.2. Slow dynamics

In this subsection, we will consider Eq. (66) at the ε^1 order. The equilibrium points correspond to $\mathscr{E} = 0$, from Eq. (27), we seek:

$$i\frac{F_0}{\alpha\mu^2} + \left(i\left(2\sigma - \frac{X_0}{\mu^2}\right) + \mu z_1\right)\varphi_1 + i\frac{X_0}{\mu^2}\varphi_2 = 0 \tag{74}$$

After substituting the equation of the SIM (see Eq. (**??**)) into Eq. (74) to eliminate the φ_1 terms, we obtain:

$$p_{10}N_2^{10} + p_8N_2^8 + p_7N_2^7 + p_6N_2^6 + p_5N_2^5 + p_4N_2^4 + p_3N_2^3 + p_2N_2^2 + p_0 = 0 \tag{75}$$

with p_j, $j = 0, ...10$ defined in Appendix E. The sets of ($\delta_2 \in \mathbb{R}$, $N_2 \in \mathbb{R}_+$ and $\sigma \in \mathbb{R}$) verifying Eq. (75) correspond to the equilibrium points of the system. The geometric position of singular points corresponds to the values of N_2 that satisfy $\det(\mathbb{B}) = 0$ (see Eq. (30)). Let us assume $X = N_2^2$ and after some mathematical developments, (see Appendix E in [38]), we obtain:

$$\det(\mathbb{B}) = a_{sv}X^2 + b_{sv}X + c_{sv} \tag{76}$$

where a_{sv}, b_{sv} and c_{sv} are defined in Appendix F. Equation 76 is identical to the equation defining the boundaries of the unstable zone of the SIM (see Eq. (73)). Figure 27 illustrates various perspectives of the equilibrium points of the system, considering the parameters from Table 4 and $\dfrac{F_0}{\alpha\mu^2} = 1.1$. In the figure, N_{qCM} is denoted as N_q ($q = 1, 2$). We can notice that there are two branches as for the constant case.

Parameter	Value
μz_1	0.1
$\dfrac{z_2}{\mu^2}$	0.1
$\dfrac{X_0}{\mu^2}$	0.5
$\dfrac{K_0}{L\mu^2}$	0.1
$\dfrac{K_{2r}}{L\mu^2}$	0.009
$\dfrac{K_{2i}}{L\mu^2}$	0.009
k_{4r}	0
k_{4i}	0
ε	0.01
L	100

Table 4: Parameters of the reduced system with a variable nonlinearity

4.3. Non-dimensionalized form of discrete equation of the chain

The non-dimensionalized equations of the discrete chain (see Eq. (32)) considering $\Lambda(v) = k_2(t)v_j^3(t)$ are as follows:

$$\begin{cases} \ddot{u}_j + \dfrac{1}{\mu}(2u_j - u_{j-1} - u_{j+1}) + \dfrac{\varepsilon z_1}{\mu}(2\dot{u}_j - \dot{u}_{j-1} - \dot{u}_{j+1}) + \dfrac{\varepsilon X_0}{\mu^2}(u_j - v_j) = \dfrac{\varepsilon F_0}{\mu^2}\cos(\mu\tau)\sin(\nu\tau) \\ \varepsilon\ddot{v}_j + \dfrac{\varepsilon P_0(\tau)}{\mu^2}v_j^3 + \dfrac{\varepsilon z_2}{\mu}\dot{v}_j - \dfrac{\varepsilon X_0}{\mu^2}(u_j - v_j) = 0 \end{cases} \tag{77}$$

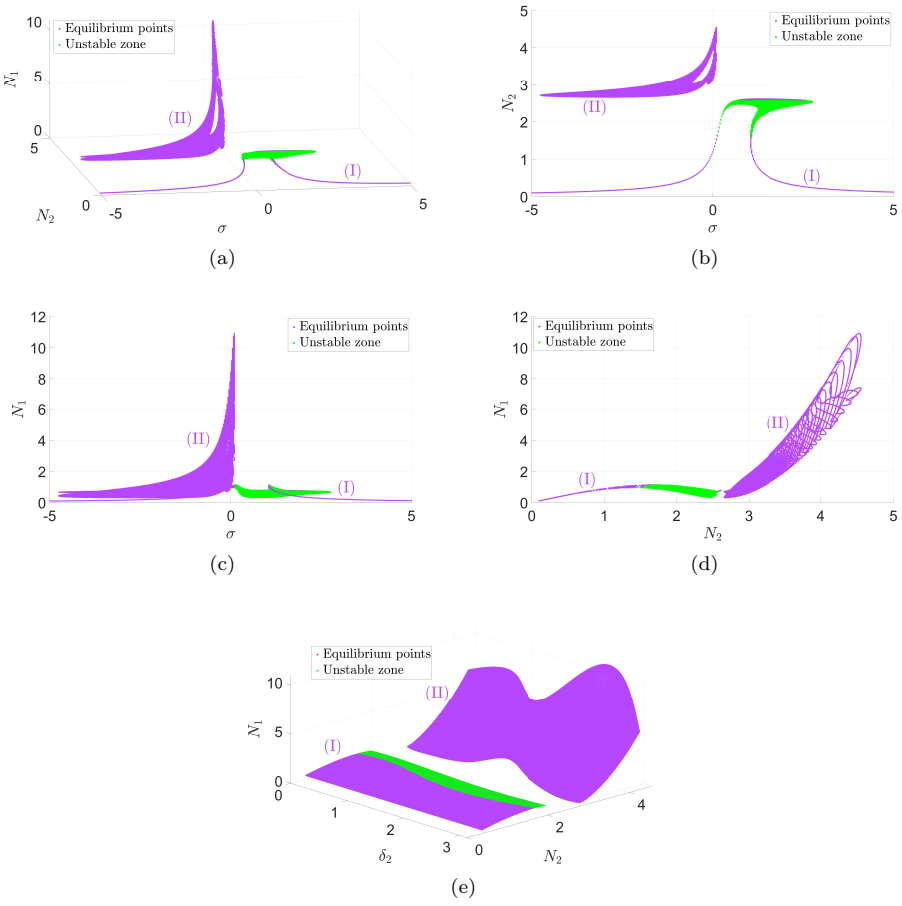

Figure 27: Equilibrium points of the reduced system with a time-dependent nonlinearity under external excitation $\frac{F_0}{\alpha\mu^2} = 1.1$, a) Three dimensional view (σ, N_2, N_1); b) Two dimensional view (σ, N_2); c) Two dimensional view (σ, N_1); d) Two dimensional view (N_2, N_1); e) Three dimensional view (δ_2, N_2, N_1), for parameters from Table 4. Equilibrium points situated in the unstable zone of the SIM are in green.

with $\varepsilon z_1 = \dfrac{c_1}{\sqrt{k_1 M}}$; $\varepsilon X_0 = \dfrac{\gamma}{k_1}$; $\varepsilon P_0(\tau) = \frac{k_2(t)}{k_1}$; $\varepsilon z_2 = \dfrac{c_2}{\sqrt{k_1 M}}$.

In the next subsection, we will numerically integrate the equations of the reduced system (see Eq. (64)) and the discrete system (see Eq. (77)) using the Runge-Kutta method. The obtained results will then be compared.

4.4. Numerical results

4.4.1. Basins of attractions

As for the constant stiffness case, we analyze the basins of attraction for the first cell (also corresponding to the basins of attractions of cell 51$^{\text{st}}$) of the discrete and continuous systems in the modal domain, as depicted in Fig. 28. Figures 28a and 28b present different perspectives of the basin of attractions for the first cell (and also for cell 51) of the discrete chain ($N_q(\tau = 0)$ as a function of σ for $q = 1$ and $q = 2$, respectively). Similarly Figs. 28c and 28d correspond to different views of the basin of attractions of the reduced system ($N_q(\tau = 0)$ as a function of σ for $q = 1$ and $q = 2$, respectively). As for the constant case (see Sect. 3.4.2) $N_1(\tau = 0)$ and $N_2(\tau = 0)$ correspond to $g(\tau = 0)$ and $h(\tau = 0)$, respectively. Red dots on the plots indicate a quasi-periodic regime, while light and dark blue dots represent periodic states (isola and main branch, respectively). The purple line represents the equilibrium points of the reduced system and the green line represents for the unstable zone of the SIM. As observed in the constant case, the behavior of the systems depends more on $N_1(\tau = 0)$ than on $N_2(\tau = 0)$, i.e. the behavior depends more on the initial displacement of the main mass than that of the mass with the nonlinearity. Here $\delta_2(\tau = 0)$ is not considered as a parameter for the basin of attractions because its depends on $h(\tau = 0)$ and $\dot{h}(\tau = 0)$, which are already considered by $N_2(\tau = 0)$. For the first cell (and also for the 51$^{\text{st}}$ cell) of the discrete chain, the quasi-periodic regime appears for $\sigma > -0.28$ which is not precise compared to the unstable zone of the SIM starting at $\sigma = 0.13$. However for the reduced system, the quasi-periodic regime agrees better with the predictions. In contrast to systems with constant nonlinearity, there is no specific zone of σ where the systems reach the isola for very low IC. For σ around -0.6 and $N_1 \in [6; 8]$ as well as $\sigma \in [-0.6; -0.1]$ and above the equilibrium points, two zones are identified where both systems are on the isola (see Figs. 28a and 28c). For the discrete chain, however, there is another zone where the first cell is on the isola: for $\sigma \in [-0.65; 0.3]$ and $N_1 \in [0; 4]$ (see Fig. 28a). It is important to note that only the basin of attractions of the first cell of the discrete chain is plotted, which does not fully represent the behavior of the entire chain. For some parameters, only the first cell or those in close to it may be on the isola while most cells remain on the main branch.

4.4.2. An example for the forced system

In this section, we focus on a representative example, specifically a forced case where the equilibrium points are positioned in the unstable zone with $\sigma = 0.5$ and $\dfrac{F_0}{\alpha\mu^2} = 1.1$. The parameters for this example are given in Table 4. Figures 29a and 29b depict a three-dimensional view of systems amplitudes (N_1 as a function of N_2 and δ_2) and a two-dimensional view (N_1 as a function of N_2), respectively. The results obtained from the reduced system are in light blue while those of the discrete system in the modal domain are in dark blue. The red curve corresponds to the SIM, the green lines represent the boundaries of its unstable zone and the pink dot denoted the IC. Figure 30 illustrates the time responses of $N_{qCM}(\tau)$, $N_{qDM}(\tau)$ and $\delta_{qDM}(\tau)$. Finally, Figs. 31 and 32 represent the responses of cells 51 and 60 of $N_{qDPh}(\tau)$, $\delta_{2DPh}(\tau)$ and $N_{qCMPh}(\tau)$, $\delta_{2CMPh}(\tau)$ for $x = 50$ and $x = 59$ ($q = 1, 2$), respectively. These figures demonstrate that both systems are in quasi-periodic regimes. As for the constant case, the amplitude and the frequency of the system during repeated bifurcations are different, but the reduced system verifies the predictions of the analytical study (see Fig. 29).
The Poincaré maps of both discrete (dark blue lines) and continuous (light blue lines) systems in the modal domain are plotted in Fig. 33. The form of the closed loop maps indicates that the different systems exhibit quasi-periodic behaviors.

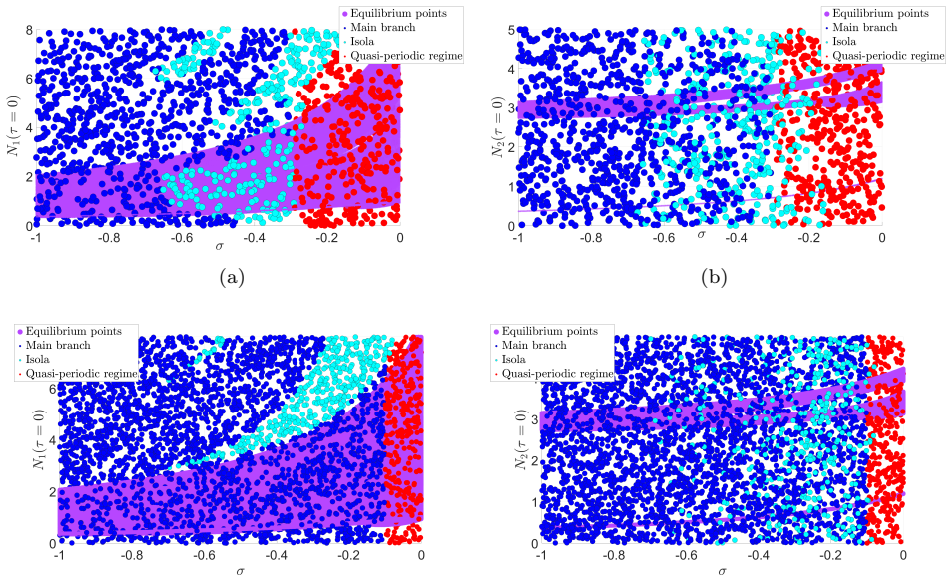

Figure 28: Basins of attractions a) $N_{1DPh,1}$ as a function of σ; b) $N_{2DPh,1}$ as a function of σ; c) N_{1CM} as a function of σ; d) N_{2CM} as a function of σ.

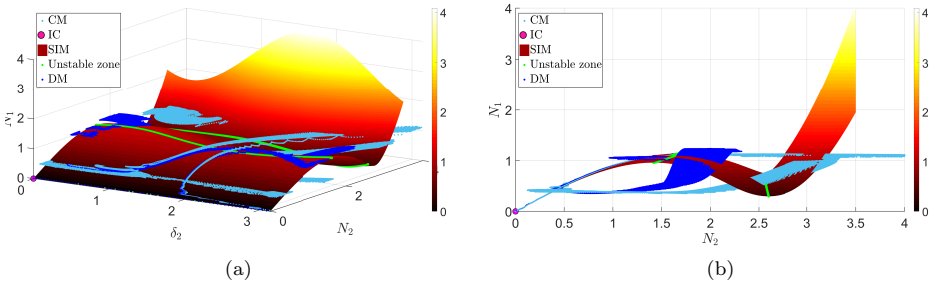

Figure 29: NI of Eq. (64) in light blue (reduced system) and Eq. (77) in dark blue (discrete system in modal domain), SIM of the reduced system (in black), its unstable zone (in green), the boundaries of the unstable zone (white dots) and the ICs (pink dot) for parameters from Table 4, $\frac{F_0}{\alpha\mu^2} = 1.1$, $\sigma = 0.5$, $(g(\tau=0), h(\tau=0), \dot{g}(\tau=0), \dot{h}(\tau=0)) = (0,0,0,0)$.

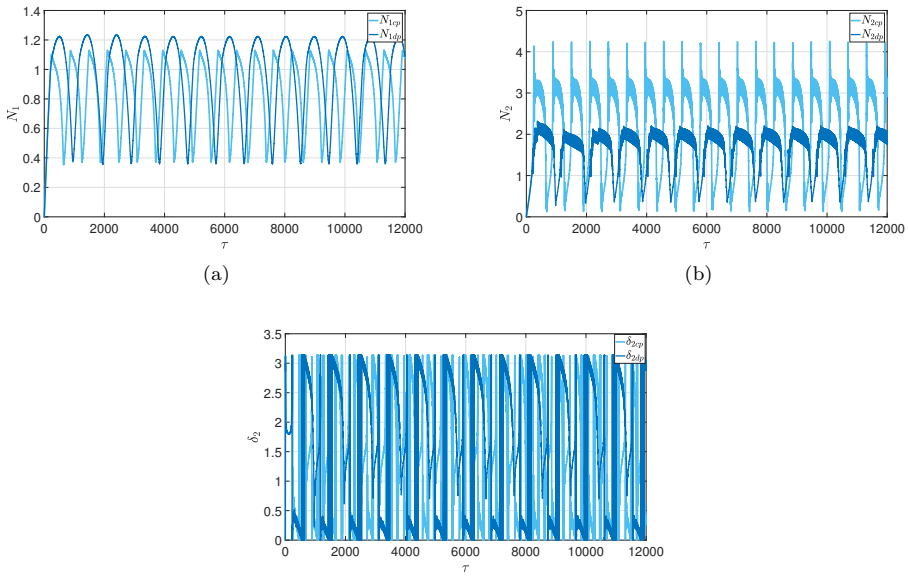

(a) (b)

(c)

Figure 30: a) N_{1DM} and N_{1CM} as functions of τ; b) N_{2DM} and N_{2CM} as functions of τ; c) δ_{2DM} and δ_{2CM} as functions of τ (dark blue and light blue, respectively); for parameters from Table 4, $\frac{F_0}{\alpha\mu^2} = 1.1$, $\sigma = 0.5$, $(g(\tau = 0), h(\tau = 0), \dot{g}(\tau = 0), \dot{h}(\tau = 0)) = (0, 0, 0, 0)$.

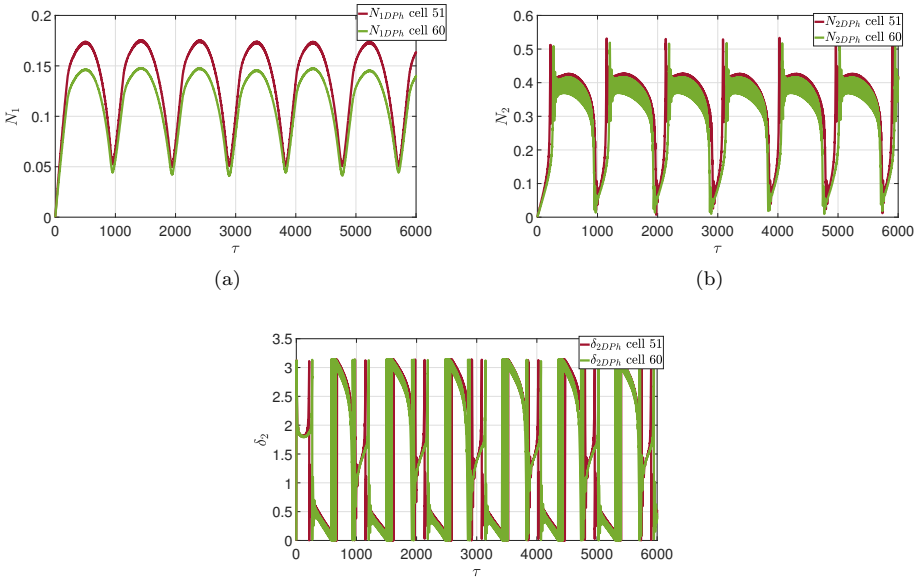

Figure 31: a) N_{1DPh} as a function of τ; b) N_{2DPh} as a function of τ of cells 51 and 60 (dark red and dark green); for parameters from Table 4, $\frac{F_0}{\alpha\mu^2} = 1.1$, $\sigma = 0.5$, $(g(\tau=0), h(\tau=0), \dot{g}(\tau=0), \dot{h}(\tau=0)) = (0,0,0,0)$.

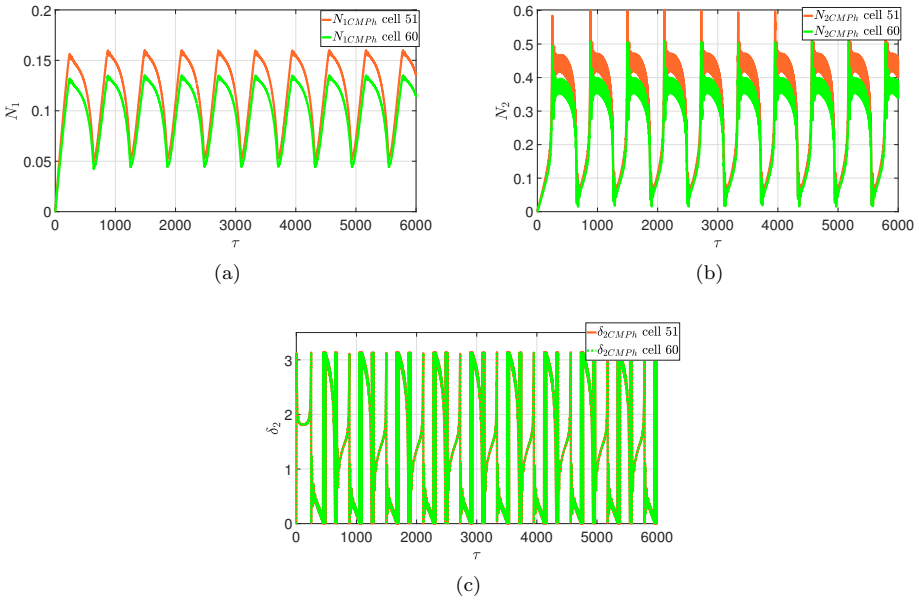

Figure 32: a) N_{1CMPh} as a function of τ; b) N_{2CMPh} as a function of τ of for $x = 50$ and $x = 59$ (orange and light green); for parameters from Table 4, $\frac{F_0}{\alpha\mu^2} = 1.1$, $\sigma = 0.5$, $(g(\tau=0), h(\tau=0), \dot{g}(\tau=0), \dot{h}(\tau=0)) = (0,0,0,0)$.

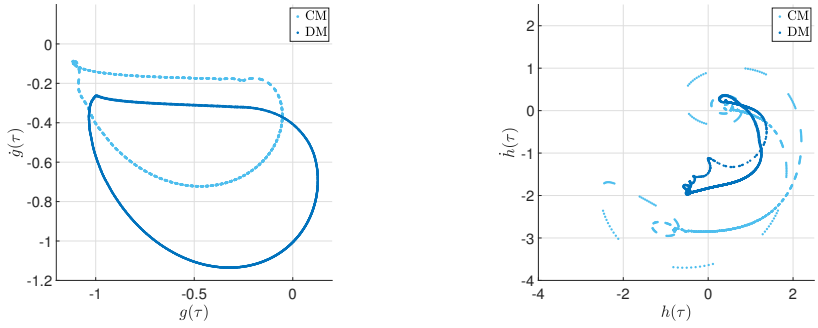

(a) (b)

Figure 33: Poincaré maps a) $\dot{g}(\tau)$ as a function of $g(\tau)$ and $\dot{g}_D(\tau)$ as a function of $g_D(\tau)$; b) $\dot{h}(\tau)$ as a function of $h(\tau)$ $\dot{h}_D(\tau)$ as a function of $h_D(\tau)$ (dark blue and light blue); for parameters from Table 4, $\frac{F_0}{\alpha\mu^2} = 1.1$, $\sigma = 0.5$, $(g(\tau=0), h(\tau=0), \dot{g}(\tau=0), \dot{h}(\tau=0)) = (0,0,0,0)$.

Then, the filtering of the first harmonic of the responses shown in Fig. 30 is presented in Fig. 34. Similar to the previous case, for N_1 only the first mode is activated and for N_2 the first and the third harmonics are activated. The filtering process helps to clarify the cause of the differences between results, since all the analytical developments are based on keeping only the first harmonics. However, the analytical developments are in good qualitative agreement with the numerical results and correctly predict different regimes of the system.

5. Conclusion

The purpose of this paper was to study the behavior of a periodic chain of coupled oscillators with a time-dependent cubic restoring forcing function, which has not been well studied. The goal was to verify that the analytical predictions of the reduced system can be used to predict the behavior of the discrete chain. This reduced system is defined from the continuous equations of the chain projected on an arbitrary mode by neglecting the internal resonances. Although this method captures the main dynamics, this approximation leads to lower accuracy and differences in response amplitude. Analytical predictions are made using the multiple scale method and complex variables of Manevitch. Different dynamics of the system are detected leading to the clarification of several possible regimes, i.e. periodic and non-periodic. Two cases are considered, the first with constant nonlinearity and the second with time-varying nonlinearity. The analytical predictions are in good qualitative agreement with results obtained from direct numerical integrations of the chain and the reduced system, although slight discrepancies between predicted and numerically obtained amplitudes are observed in some cases.

Nevertheless, the predicted regimes (periodic or non-periodic) from analytical developments agree well with those observed in the chain. The results of this study provide tools for the development of new types of time-dependent (meta-) materials for vibro-acoustic control. One perspective of this work is the consideration of internal resonances of the chain [34, 50] and also the programming/or fabrication of time-dependent nonlinearities for an experimental study [51]. Moreover, in the current study, we have assumed that the oscillators are perfectly identical and we do not include uncertainties in the design [19, 52]. To take into account of the uncertainties required for experimental studies, a stochastic optimization procedure should be performed. This study is also a perspective of the current work.

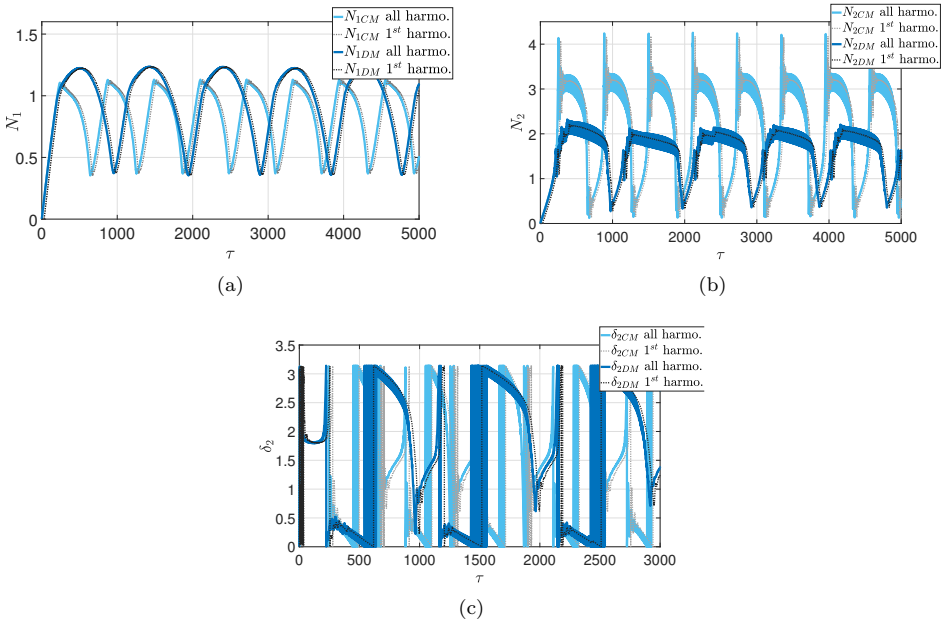

Figure 34: Filtering around the first harmonic and the response with all the harmonics a) N_{1DM} and N_{1CM} as functions of τ; b) N_{2DM} and N_{2CM} as functions of τ (black dotted line, dark blue line, gray dotted line and light blue line, respectively); for parameters from Table 4, $\frac{F_0}{\alpha\mu^2} = 1.1$, $\sigma = 0.5$, $(g(\tau=0), h(\tau=0), \dot{g}(\tau=0), \dot{h}(\tau=0)) = (0,0,0,0)$.

Acknowledgements

The authors would like to thank the following organizations for supporting this research: (i) The "Ministère de la transition écologique" and (ii) LABEX CELYA (ANR-10-LABX-0060) of the "Université de Lyon" within the program "Investissement d'Avenir"(ANR-11-IDEX-0007) operated by the French National Research Agency (ANR).

Declaration

Conflict of interest: The authors declare that they have no conflict of interest.

Appendix A. Parameter of the equation of the equilibrium point for constant cubic nonlinearity

$$a_c = \left(\frac{3}{4L\mu_k^2}P_0\right)^2\left[(\mu_k z_1)^2 + (2\sigma - \frac{X_0}{\mu_k^2})^2\right] \tag{A.1}$$

$$b_c = \frac{3}{2L\mu_k^2}P_0\left[(-1+\frac{X_0}{\mu_k^2})\left[(\mu_k z_1)^2 + (2\sigma_- \frac{X_0}{\mu_k^2})^2\right] + (2\sigma - \frac{X_0}{\mu_k^2})\frac{X_0^2}{\mu_k^4}\right] \tag{A.2}$$

$$\begin{aligned} c_c = (-1+\frac{X_0}{\mu_k^2})^2\left[(\mu_k z_1)^2 + (2\sigma - \frac{X_0}{\mu_k^2})^2\right] + 2(-1+\frac{X_0}{\mu_k^2})(2\sigma - \frac{X_0}{\mu_k^2})\frac{X_0^2}{\mu_k^4} \\ + \left(z_1 z_2 + \frac{X_0^2}{\mu_k^4}\right)^2 + (2\sigma - \frac{X_0}{\mu_k^2})^2\frac{z_2^2}{\mu_k^2} \end{aligned} \tag{A.3}$$

$$d_c = -F_0^2\frac{X_0^2}{\alpha\mu_k^6} \tag{A.4}$$

Appendix B. Details of the SIM for a time-varying nonlinearity

$$A = \left(-1+\frac{X_0}{\mu_k^2}\right) - \frac{N_2^2}{4L\mu_k^2}\left(4K_{2R}\cos(2\delta_2) + 4K_{2I}\sin(2\delta_2) - 3K_0 - K_{4R}\cos(4\delta_2) - K_{4I}\sin(4\delta_2)\right) \tag{B.1}$$

$$B = \frac{z_2}{\mu_k} - \frac{N_2^2}{4L\mu_k^2}\left(-2K_{2R}\sin(2\delta_2) + 2K_{2I}\cos(2\delta_2) + K_{4R}\sin(4\delta_2) - K_{4I}\cos(4\delta_2)\right) \tag{B.2}$$

Appendix C. Parameters of $\mathbb{M}_v$ for a time-varying nonlinearity

We have $\mathbb{M}_v = \begin{pmatrix}\mathbb{M}_{v11} & \mathbb{M}_{v12}\\ \mathbb{M}_{v21} & \mathbb{M}_{v22}\end{pmatrix}$ and

$$\begin{cases} \mathbb{M}_{v11} = & -\frac{i}{2}\left(1 - \frac{X_0}{\mu_k^2} + \frac{3}{4L\mu_k^2}\left[\varphi_2^2 K_2^* - 2\varphi_2\varphi_2^* K_0 + \varphi_2^{*2}K_2\right]\right) - \frac{z_2}{2\mu_k} \\ \mathbb{M}_{v12} = & -\frac{3i}{8L\mu_k^2}\left(-\varphi_2^2 K_0 + 2\varphi_2\varphi_2^* K_2 - \varphi_2^{*2}K_4\right) \\ \mathbb{M}_{v21} = & \frac{3i}{8L\mu_k^2}\left(-\varphi_2^{*2} K_0 + 2\varphi_2\varphi_2^* K_2^* - \varphi_2^2 K_4^*\right) \\ \mathbb{M}_{v22} = & \frac{i}{2}\left(1 - \frac{X_0}{\mu_k^2} + \frac{3}{4L\mu_k^2}\left[\varphi_2^{*2} K_2 - 2\varphi_2\varphi_2^* K_0 + \varphi_2^2 K_2^*\right]\right) - \frac{z_2}{2\mu_k} \end{cases} \tag{C.1}$$

Appendix D. Parameters of the equation of the unstable zone of the SIM for a time-varying nonlinearity

$$
\begin{aligned}
a_v = \frac{9}{64L\mu_k^2}(&3K_0^2 - 2K_{2I}^2 - 2K_{2R}^2 - K_{4I}^2 - K_{4R}^2 + \\
&4(-K_0K_{2R} + K_{2I}K_{4I} + K_{2R}K_{4R})\cos(2\delta_2) - 2(K_{2I}^2 - K_{2R}^2 + K_0K_{4R})\cos(4\delta_2) \\
&- 4(-K_{2R}K_{4I} + K_{2I}(K_0 + K_{4R}))\sin(2\delta_2) + 2(2K_{2I}K_{2R} - K_0K_{4I})\sin(4\delta_2))
\end{aligned} \tag{D.1}
$$

$$
b_v = \frac{3}{4L\mu_k^2}\left(-1 + \frac{X_0}{\mu_k^2}\right)(K_0 - K_{2R}\cos(2\delta_2) - K_{2I}\sin(2\delta_2)) \tag{D.2}
$$

$$
c_v = \frac{1}{4}((-1 + \frac{X_0}{\mu_k^2})^2 + \frac{z_2^2}{\mu_k^2}) \tag{D.3}
$$

Appendix E. Parameters of the equation of equilibrium points for a time-varying nonlinearity

$$
\begin{aligned}
p_{10} = -\frac{9}{L\mu_k^2}((&\frac{X_0}{\mu_k^2} - 2\sigma)^2 + (\mu_k z_1)^2)^2(9K_0^4 + K_0(8K_{2I}K_{2R}K_{4I} - 4K_{2I}^2K_{4R} + 4K_{2R}^2K_{4R}) \\
&+ (K_{2I}^2 + K_{2R}^2)(8K_{2I}^2 + 8K_{2R}^2 - K_{4I}^2 - K_{4R}^2) - K_0^2(19K_{2I}^2 + 19K_{2R}^2 + K_{4I}^2 + K_{4R}^2) \\
&- 2(K_0^2(K_{2I}K_{4I} - K_{2R}K_{4R}) + (K_{2I}^2 + K_{2R}^2)(K_{2I}K_{4I} - K_{2R}K_{4R}) \\
&+ K_0(-3K_{2I}^2K_{2R} + K_{2R}^3 - K_{2R}K_{4I}^2 + 2K_{2I}K_{4I}K_{4R} + K_{2R}K_{4R}^2))\cos(6\delta_2) \\
&+ 2(K_0^2(K_{2R}K_{4I} + K_{2I}K_{4R}) + (K_{2I}^2 + K_{2R}^2)(K_{2R}K_{4I} + K_{2I}K_{4R}) \\
&+ K_0(K_{2I}^3 - 2K_{2R}K_{4I}K_{4R} + K_{2I}(-3K_{2R}^2 - K_{4I}^2 + K_{4R}^2))))\sin(6\delta_2)
\end{aligned} \tag{E.1}
$$

$$
p_8 = p_{81} + p_{82} \tag{E.2}
$$

with

$$
\begin{aligned}
p_{81} = \frac{24}{L\mu_k^2}((\frac{X_0}{\mu_k^2} - 2\sigma)^2 + (\mu_k z_1)^2)(\frac{X_0}{\mu_k^2}(-(18K_0^3 + 4K_{2I}K_{2R}K_{4I} \\
- 2K_{2I}^2K_{4R} + 2K_{2R}^2K_{4R} - K_0(19K_{2I}^2 + 19K_{2R}^2 + K_{4I}^2 + K_{4R}^2))(4\sigma(1+\sigma) \\
+ (\mu_k z_1)^2) - 8(K_{2I}^2K_{4I} - K_{2R}^2K_{4I} + 2K_{2I}K_{2R}K_{4R})\sigma\frac{z_2}{\mu_k}) \\
+ (4\sigma^2 + (\mu_k z_1)^2)(18K_0^3 - K_0(19K_{2I}^2 + 19K_{2R}^2 + K_{4I}^2 + K_{4R}^2) - 2K_{2I}^2(K_{4R} \\
- K_{4I}\frac{z_2}{\mu_k}) + 2K_{2R}^2(K_{4R} - K_{4I}\frac{z_2}{\mu_k}) + 4K_{2I}K_{2R}(K_{4I} \\
+ K_{4R}\frac{z_2}{\mu_k})) + \frac{X_0}{\mu_k^2}^2(18K_0^3(1+2\sigma) - K_0(19K_{2I}^2 + 19K_{2R}^2 \\
+ K_{4I}^2 + K_{4R}^2)(1+2\sigma) + 2K_{2R}^2(K_{4R} + 2K_{4R}\sigma - K_{4I}(\mu_k z_1 + \frac{z_2}{\mu_k})) \\
+ 2K_{2I}^2(-K_{4R}(1+2\sigma) + K_{4I}(\mu_k z_1 + \frac{z_2}{\mu_k})) + 4K_{2I}K_{2R}(K_{4I} + 2K_{4I}\sigma \\
+ K_{4R}(\mu_k z_1 + \frac{z_2}{\mu_k}))) + (\frac{X_0}{\mu_k^2}(-(3K_{2I}^2K_{2R} - \\
2K_{2I}K_{4I}(K_0 + K_{4R}) - K_{2R}(K_{2R}^2 - K_{4I}^2 - 2K_0K_{4R} + K_{4R}^2))(4\sigma(1+\sigma) + (\mu_k z_1)^2) \\
- 4(K_{2I}^3 + 2K_{2R}K_{4I}K_{4R} + K_{2I}(-3K_{2R}^2 + K_{4I}^2 - K_{4R}^2))\sigma\frac{z_2}{\mu_k}) \\
+ (4\sigma^2 + (\mu_k z_1)^2)(3K_{2I}^2K_{2R} - 2K_{2I}K_{4I}(K_0 + K_{4R}) + K_{2I}^3\frac{z_2}{\mu_k} \\
+ K_{2I}(-3K_{2R}^2 + K_{4I}^2 - K_{4R}^2)\frac{z_2}{\mu_k} + K_{2R}(-K_{2R}^2 + K_{4I}^2 + 2K_0K_{4R} - K_{4R}^2 + \\
2K_{4I}K_{4R}\frac{z_2}{\mu_k})) + \frac{X_0}{\mu_k^2}^2(3K_{2I}^2(K_{2R} + 2K_{2R}\sigma) + K_{2I}^3(\mu_k z_1 \\
+ \frac{z_2}{\mu_k}) + K_{2R}(-K_{2R}^2(1+2\sigma) + K_{4I}^2(1+2\sigma) - K_{4R}(-2K_0 + K_{4R})(1+2\sigma) \\
+ 2K_{4I}K_{4R}(\mu_k z_1 + \frac{z_2}{\mu_k})) - K_{2I}(2K_0(K_{4I} + 2K_{4I}\sigma) + 2K_{4I}(K_{4R} + 2K_{4R}\sigma) \\
- K_{4I}^2(\mu_k z_1 + \frac{z_2}{\mu_k}) + (3K_{2R}^2 + K_{4R}^2)(\mu_k z_1 + \frac{z_2}{\mu_k})))) \cos(6\delta_2) \quad \text{(E.3)}
\end{aligned}
$$

$$
\begin{aligned}
p_{82} = (-\frac{X_0}{\mu_k^2}((K_{2I}^3 + 2K_{2R}K_{4I}(K_0 - K_{4R}) + K_{2I}(-3K_{2R}^2 - K_{4I}^2 \\
+ 2K_0K_{4R} + K_{4R}^2))(4\sigma(1+\sigma) + (\mu_k z_1)^2) + 4(-3K_{2I}^2K_{2R} - 2K_{2I}K_{4I}K_{4R} \\
+ K_{2R}(K_{2R}^2 + K_{4I}^2 - K_{4R}^2))\sigma\frac{z_2}{\mu_k}) + \frac{X_0}{\mu_k^2}^2(K_{2I}^3(1+2\sigma) \\
- 3K_{2I}^2K_{2R}(\mu_k z_1 + \frac{z_2}{\mu_k}) - K_{2I}(K_{4I}^2(1+2\sigma) - K_{4R}(2K_0 + K_{4R})(1+2\sigma) \\
+ K_{2R}^2(3+6\sigma) + 2K_{4I}K_{4R}(\mu_k z_1 + \frac{z_2}{\mu_k})) + K_{2R}(2K_0(K_{4I} + 2K_{4I}\sigma) \\
- 2K_{4I}(K_{4R} + 2K_{4R}\sigma) + K_{4I}^2(\mu_k z_1 + \frac{z_2}{\mu_k}) + (K_{2R} - K_{4R})(K_{2R} + K_{4R})(\mu_k z_1 + \frac{z_2}{\mu_k}))) \\
+ (4\sigma^2 + (\mu_k z_1)^2)(K_{2I}^3 + 2K_{2R}K_{4I}(K_0 - K_{4R}) - 3K_{2I}^2K_{2R}\frac{z_2}{\mu_k} \\
+ K_{2R}(K_{2R}^2 + K_{4I}^2 - K_{4R}^2)\frac{z_2}{\mu_k} + K_{2I}(-3K_{2R}^2 + K_{4R}(2K_0 + K_{4R}) \\
- K_{4I}(K_{4I} + 2K_{4R}\frac{z_2}{\mu_k})))) \sin(6\delta_2) \quad \text{(E.4)}
\end{aligned}
$$

$$
\begin{aligned}
p_7 = 72\frac{F_0}{\alpha\mu_k^4 L}\frac{X_0}{\mu_k^2}((\frac{X_0}{\mu_k^2} - 2\sigma)^2 + (\mu_k z_1)^2)(((K_0^2(K_{2R} - K_{4R}) + (K_{2I}^2 + K_{2R}^2)(K_{2R} - K_{4R}) \\
- 2K_0(K_{2I}(K_{2I} + K_{4I}) + K_{2R}(-K_{2R} + K_{4R})))(\frac{X_0}{\mu_k^2} - 2\sigma) \\
+ (K_0^2(K_{2I} + K_{4I}) + (K_{2I}^2 + K_{2R}^2)(K_{2I} + K_{4I}) - 2K_0K_{2R}(2K_{2I} + K_{4I}) \\
+ 2K_0K_{2I}K_{4R})\mu_k z_1)\cos(3\delta_2) + ((K_0^2(K_{2I} - K_{4I}) \\
+ (K_{2I}^2 + K_{2R}^2)(K_{2I} - K_{4I}) - 2K_0K_{2R}K_{4I} + 2K_0K_{2I}(2K_{2R} \\
+ K_{4R}))(\frac{X_0}{\mu_k^2} - 2\sigma) - (2K_0K_{2I}(K_{2I} - K_{4I}) + K_0^2(K_{2R} + K_{4R}) - 2K_0K_{2R}(K_{2R} + K_{4R}) \\
+ (K_{2I}^2 + K_{2R}^2)(K_{2R} + K_{4R}))\mu_k z_1)\sin(3\delta_2) \quad \text{(E.5)}
\end{aligned}
$$

$$
\begin{aligned}
p_6 = -\frac{16}{L\mu_k^2}\Big(\frac{X_0}{\mu_k^2}^2\Big(-\big(-54K_0^2+19K_{2I}^2+19K_{2R}^2+K_{4I}^2+K_{4R}^2\big)\\
(8\sigma^2(3+2\sigma(3+\sigma))+2(1+6\sigma+4\sigma^2)(\mu_k z_1)^2+(\mu_k z_1)^4)\\
-2\big(-18K_0^2+19K_{2I}^2+19K_{2R}^2+K_{4I}^2+K_{4R}^2\big)\mu_k z_1(4\sigma^2+(\mu_k z_1)^2)\frac{z_2}{\mu_k}-\\
2\big(-18K_0^2+19K_{2I}^2+19K_{2R}^2+K_{4I}^2+K_{4R}^2\big)(12\sigma^2+(\mu_k z_1)^2)\frac{z_2^2}{\mu_k^2})\\
+(4\sigma^2+(\mu_k z_1)^2)^2\big(-\big(19K_{2I}^2+19K_{2R}^2+K_{4I}^2+K_{4R}^2\big)(1+\frac{z_2^2}{\mu_k^2})\\
+18K_0^2(3+\frac{z_2^2}{\mu_k^2})\big)+2\frac{X_0}{\mu_k^2}^3\big(\big(19K_{2I}^2+19K_{2R}^2+K_{4I}^2+\\
K_{4R}^2\big)\big((1+2\sigma)(4\sigma(1+\sigma)+(\mu_k z_1)^2)+4\sigma\mu_k z_1\frac{z_2}{\mu_k}\\
+4\sigma\frac{z_2^2}{\mu_k^2}\big)-18K_0^2(3(1+2\sigma)(4\sigma(1+\sigma)+(\mu_k z_1)^2)+\\
4\sigma\mu_k z_1\frac{z_2}{\mu_k}+4\sigma\frac{z_2^2}{\mu_k^2})\big)+\frac{X_0}{\mu_k^2}^4\\
\big(-\big(19K_{2I}^2+19K_{2R}^2+K_{4I}^2+K_{4R}^2\big)(1+4\sigma(1+\sigma)+(\mu_k z_1+\frac{z_2}{\mu_k})^2)\\
+18K_0^2(3+12\sigma(1+\sigma)+(\mu_k z_1+\frac{z_2}{\mu_k})^2)\big)-2\frac{X_0}{\mu_k^2}(4\sigma^2+\\
(\mu_k z_1)^2)\big(-\big(19K_{2I}^2+19K_{2R}^2+K_{4I}^2+K_{4R}^2\big)((\mu_k z_1)^2+4\sigma(1+\sigma+\\
\frac{z_2^2}{\mu_k^2}))+18K_0^2(3(\mu_k z_1)^2+4\sigma(3+3\sigma+\frac{z_2^2}{\mu_k^2}))\big)\\
-2\big((\frac{X_0}{\mu_k^2}-2\sigma)^2+(\mu_k z_1)^2\big)\big((4\sigma^2+(\mu_k z_1)^2)(1+\frac{z_2^2}{\mu_k^2})\\
+\frac{X_0}{\mu_k^2}^2(1+4\sigma(1+\sigma)+(\mu_k z_1+\frac{z_2}{\mu_k})^2)\\
-2\frac{X_0}{\mu_k^2}((\mu_k z_1)^2+2\sigma(1+2\sigma+\frac{z_2^2}{\mu_k^2}))\big)\\
((K_{2I}K_{4I}-K_{2R}K_{4R})\cos(6\delta_2])-(K_{2R}K_{4I}+K_{2I}K_{4R})\sin(6\delta_2)))
\end{aligned}
\tag{E.6}
$$

$$
p_5 = p_{51} + p_{52} \tag{E.7}
$$

$$
\begin{aligned}
p_{51} = 192\frac{F_0}{\alpha\mu_k^4 L}\frac{X_0}{\mu_k^2}((\frac{X_0}{\mu_k^2})^3 (K_{2I}^2(1+2\sigma) - K_0(K_{2R}-K_{4R})(1+2\sigma) \\
- K_{2R}(K_{2R}-K_{4R}+2K_{2R}\sigma-2K_{4R}\sigma+K_{4I}(\mu_k z_1+\frac{z_2}{\mu_k})) + K_{2I}(K_{4I} \\
+ 2K_{4I}\sigma-(2K_{2R}-K_{4R})(\mu_k z_1+\frac{z_2}{\mu_k}))) - (4\sigma^2+(\mu_k z_1)^2)(K_0(-2K_{2R}\sigma \\
+ 2K_{4R}\sigma+K_{4I}\mu_k z_1) + K_{2I}^2(2\sigma - z_1 z_2) - K_{2R}(2K_{2R}\sigma-2K_{4R}\sigma+K_{4I}\mu_k z_1 \\
+ 2K_{4I}\sigma\frac{z_2}{\mu_k} - K_{2R}z_1 z_2 + K_{4R}z_1 z_2) + K_{2I}((K_0-2K_{2R}+K_{4R})\mu_k z_1 + 2(-2K_{2R} \\
+ K_{4R})\sigma\frac{z_2}{\mu_k} + K_{4I}(2\sigma - z_1 z_2))) - (\frac{X_0}{\mu_k^2})^2 (K_0(-2(K_{2R} \\
- K_{4R})\sigma(3+4\sigma) + K_{4I}\mu_k z_1 + 2K_{4I}\sigma\mu_k z_1 + (-K_{2R}+K_{4R})(\mu_k z_1)^2) \\
+ K_{2I}^2(6\sigma+8\sigma^2-\mu_k z_1 z_2) - K_{2R}(2(K_{2R}-K_{4R})\sigma(3+4\sigma) + K_{4I}z_1 + 4K_{4I}\sigma\mu_k z_1 \\
+ 6K_{4I}\sigma\frac{z_2}{\mu_k} + (-K_{2R}+K_{4R})z_1 z_2) + K_{2I}(K_0(\mu_k z_1 + 2\sigma\mu_k z_1) \\
- (2K_{2R}-K_{4R})(\mu_k z_1 + 4\sigma\mu_k z_1 + 6\sigma\frac{z_2}{\mu_k}) + K_{4I}(6\sigma+8\sigma^2 - z_1 z_2))) \\
+ \frac{X_0}{\mu_k^2}(K_0(-4(K_{2R}-K_{4R})\sigma^2(3+2\sigma) + 4K_{4I}\sigma(1+\sigma)\mu_k z_1 \\
- (K_{2R}-K_{4R})(1+2\sigma)(\mu_k z_1)^2 + K_{4I}(\mu_k z_1)^3) + K_{2I}^2((\mu_k z_1)^2 + 2\sigma(6\sigma+4\sigma^2 \\
+ \mu_k z_1(\mu_k z_1 - 2\frac{z_2}{\mu_k}))) + K_{2I}((K_0-2K_{2R}+K_{4R})\mu_k z_1(4\sigma(1+\sigma) \\
+ (\mu_k z_1)^2) + K_{4I}((\mu_k z_1)^2 + 2\sigma(6\sigma+4\sigma^2+\mu_k z_1(\mu_k z_1 - 2\frac{z_2}{\mu_k}))) \\
- (2K_{2R}-K_{4R})(12\sigma^2+(\mu_k z_1)^2)\frac{z_2}{\mu_k}) - K_{2R}(K_{2R}((\mu_k z_1)^2 \\
+ 2\sigma(6\sigma+4\sigma^2+\mu_k z_1(\mu_k z_1 - 2\frac{z_2}{\mu_k}))) - K_{4R}((\mu_k z_1)^2 + 2\sigma(6\sigma+4\sigma^2 \\
+ \mu_k z_1(\mu_k z_1 - 2\frac{z_2}{\mu_k}))) + K_{4I}(4\sigma\mu_k z_1 + (\mu_k z_1)^2(\mu_k z_1 + \frac{z_2}{\mu_k}) \\
+ 4\sigma^2(\mu_k z_1 + 3\frac{z_2}{\mu_k}))))) \cos(3\delta_2) \quad \text{(E.8)}
\end{aligned}
$$

$$
\begin{aligned}
p_{52} = \frac{1}{L\mu_k^2}\Big(\frac{X_0^3}{\mu_k^6}\Big(&-K_0(K_{2I}-K_{4I})(1+2\sigma) - K_{2I}^2(\mu_k z_1 + \frac{z_2}{\mu_k}) \\
&- K_{2I}(K_{4R} + 2(K_{2R} + 2K_{2R}\sigma + K_{4R}\sigma) - K_{4I}(\mu_k z_1 \\
&+ \frac{z_2}{\mu_k})) + K_{2R}(K_{4I} \\
&+ 2K_{4I}\sigma + (K_{2R}+K_{4R})(\mu_k z_1 + \frac{z_2}{\mu_k}))) + (4\sigma^2 + (\mu_k z_1)^2)(2K_0(K_{2I}-K_{4I})\sigma \\
&+ K_0(K_{2R}+K_{4R})\mu_k z_1 + K_{2I}^2(\mu_k z_1 + 2\sigma\frac{z_2}{\mu_k}) + K_{2I}(4K_{2R}\sigma \\
&+ 2K_{4R}\sigma - K_{4I}\mu_k z_1 - (2K_{4I}\sigma + (2K_{2R}+K_{4R})\mu_k z_1)\frac{z_2}{\mu_k}) \\
&- K_{2R}((K_{2R}+K_{4R})(\mu_k z_1 + 2\sigma\frac{z_2}{\mu_k}) + K_{4I}(2\sigma - z_1 z_2))) \\
&+ \frac{X_0^2}{\mu_k^4}(K_0(2(K_{2I}-K_{4I})\sigma(3+4\sigma) + (K_{2R}+K_{4R})(1+2\sigma)\mu_k z_1 \\
&+ (K_{2I}-K_{4I})(\mu_k z_1)^2) + K_{2I}^2(\mu_k z_1 + 4\sigma\mu_k z_1 + 6\sigma\frac{z_2}{\mu_k}) \\
&+ K_{2I}(2(2K_{2R}+K_{4R})\sigma(3+4\sigma) - K_{4I}\mu_k z_1 - 4K_{4I}\sigma\mu_k z_1 \\
&- (6K_{4I}\sigma + (2K_{2R}+K_{4R})\mu_k z_1)\frac{z_2}{\mu_k}) - K_{2R}((K_{2R}+K_{4R})(\mu_k z_1 + \\
&4\sigma\mu_k z_1 + 6\sigma\frac{z_2}{\mu_k}) + K_{4I}(6\sigma + 8\sigma^2 - z_1 z_2))) + \frac{X_0}{\mu_k^2}(K_0(-4(K_{2I} \\
&- K_{4I})\sigma^2(3+2\sigma) - 4(K_{2R}+K_{4R})\sigma(1+\sigma)\mu_k z_1 - (K_{2I}-K_{4I})(1+2\sigma)(\mu_k z_1)^2 \\
&- (K_{2R}+K_{4R})(\mu_k z_1)^3) + K_{2I}(-4(2K_{2R}+K_{4R})\sigma^2(3+2\sigma) + 4K_{4I}\sigma(1+\sigma)\mu_k z_1 \\
&- (2K_{2R}+K_{4R})(1+2\sigma)(\mu_k z_1)^2 + K_{4I}(\mu_k z_1)^3 + 4(2K_{2R}+K_{4R})\sigma z_1 z_2 \\
&+ K_{4I}(12\sigma^2 + (\mu_k z_1)^2)\frac{z_2}{\mu_k}) - K_{2I}^2(4\sigma\mu_k z_1 + (\mu_k z_1)^2(\mu_k z_1 \\
&+ \frac{z_2}{\mu_k}) + 4\sigma^2(\mu_k z_1 + 3\frac{z_2}{\mu_k})) + K_{2R}(K_{4I}((\mu_k z_1)^2 + 2\sigma(6\sigma + 4\sigma^2 + \\
&\mu_k z_1(\mu_k z_1 - 2\frac{z_2}{\mu_k}))) + (K_{2R}+K_{4R})(4\sigma\mu_k z_1 \\
&+ (\mu_k z_1)^2(\mu_k z_1 + \frac{z_2}{\mu_k}) + 4\sigma^2(\mu_k z_1 + 3\frac{z_2}{\mu_k}))))\Big)\sin(3\delta_2) \qquad \text{(E.9)}
\end{aligned}
$$

$$
\begin{aligned}
p_4 = -128(2(4\sigma^2 + (\mu_k z_1)^2)^2(1 + \frac{z_2^2}{\mu_k^2})^2 - 8\frac{X_0}{\mu_k^2}(4\sigma^2 + \\
(\mu_k z_1)^2)(1 + \frac{z_2^2}{\mu_k^2})((\mu_k z_1)^2 + 2\sigma(1 + 2\sigma + \frac{z_2^2}{\mu_k^2})) + \frac{X_0^4}{\mu_k^8}(3\frac{F_0^2}{\alpha^2\mu_k^4}(\frac{K_0}{L\mu_k^2} + \frac{K_{2R}}{L\mu_k^2} \\
+ \frac{2}{L\mu_k^2}(K_0 + K_{2R})\sigma + \frac{K_{2I}}{L\mu_k^2}(\mu_k z_1 + \frac{z_2}{\mu_k})) \\
+ 2(1 + 4\sigma(1 + \sigma) + (\mu_k z_1 + \frac{z_2}{\mu_k})^2)^2) + \frac{X_0^2}{\mu_k^4}(192\sigma^3 \\
(1 + \frac{z_2^2}{\mu_k^2}) + 64\sigma^4(3 + \frac{z_2^2}{\mu_k^2}) + 12\sigma\mu_k z_1(\frac{F_0^2}{\alpha^2\mu_k^4 L\mu_k^2}(K_{2I} \\
- K_{2R}\frac{z_2}{\mu_k}) + 4\mu_k z_1(1 + \frac{z_2^2}{\mu_k^2})) + 4\sigma^2(3\frac{F_0^2}{\alpha^2\mu_k^4 L\mu_k^2} \\
(K_0 + K_{2R} + K_{2I}\frac{z_2}{\mu_k}) + 12(1 + \frac{z_2^2}{\mu_k^2})^2 + 8(\mu_k z_1)^2(3 + v) + 8\mu_k z_1(\frac{z_2}{\mu_k} \\
+ \frac{z_2^3}{\mu_k^3})) + (\mu_k z_1)^2(4 + 12(\mu_k z_1)^2 + 3\frac{F_0^2}{\alpha^2\mu_k^4 L\mu_k^2} \\
(K_0 - K_{2R} - K_{2I}\frac{z_2}{\mu_k}) + 4\frac{z_2}{\mu_k}(\mu_k z_1 \\
+ \frac{z_2}{\mu_k})(2 + \frac{z_2}{\mu_k}(\mu_k z_1 + \frac{z_2}{\mu_k})))) - \frac{X_0^3}{\mu_k^6}(128\sigma^4 \\
+ 64\sigma^3(3 + \frac{z_2^2}{\mu_k^2}) + 4\sigma^2(3\frac{F_0^2}{\alpha^2\mu_k^4 L\mu_k^2}(K_0 + K_{2R}) \\
+ 8(3 + 2(\mu_k z_1)^2 + 2z_1 z_2 + 3\frac{z_2^2}{\mu_k^2})) + \mu_k z_1(8\mu_k z_1(1 + (\mu_k z_1 + \frac{z_2}{\mu_k})^2) \\
+ 3\frac{F_0^2}{\alpha^2\mu_k^4 L\mu_k^2}(2K_{2I} + K_0\mu_k z_1 - K_{2R}(\mu_k z_1 + 2\frac{z_2}{\mu_k}))) \\
+ 4\sigma(3\frac{F_0^2}{\alpha^2\mu_k^4}(\frac{K_0}{L\mu_k^2} + \frac{K_{2R}}{L\mu_k^2} + \frac{K_{2I}}{L\mu_k^2}(\mu_k z_1 \\
+ \frac{z_2}{\mu_k})) + 4((1 + \frac{z_2^2}{\mu_k^2})^2 + (\mu_k z_1)^2(3 + \frac{z_2^2}{\mu_k^2}) + 2\mu_k z_1(\frac{z_2}{\mu_k} + \frac{z_2^3}{\mu_k^3}))))) \quad \text{(E.10)}
\end{aligned}
$$

$$
\begin{aligned}
p_3 = 128\frac{F_0}{\alpha\mu_k^2}\frac{X_0}{\mu_k^2}((4\sigma^2 + (\mu_k z_1)^2)(1 + \frac{z_2^2}{\mu_k^2}) + \frac{{X_0}^2}{\mu_k^2}(1 + 4\sigma(1 + \sigma) + (\mu_k z_1 + \frac{z_2}{\mu_k})^2) \\
- 2\frac{X_0}{\mu_k^2}((\mu_k z_1)^2 + 2\sigma(1 + 2\sigma + \frac{z_2^2}{\mu_k^2})))(((\frac{K_{2R}}{L\mu_k^2} - \frac{K_{4R}}{L\mu_k^2})(\frac{X_0}{\mu_k^2} - 2\sigma) + (\frac{K_{2I}}{L\mu_k^2} + \frac{K_{4I}}{L\mu_k^2})\mu_k z_1)\cos(3\delta_2) \\
+ ((\frac{K_{2I}}{L\mu_k^2} - \frac{K_{4I}}{L\mu_k^2})(\frac{X_0}{\mu_k^2} - 2\sigma) - \frac{1}{L\mu_k}(K_{2R} + K_{4R})z_1)\sin(3\delta_2)) \quad \text{(E.11)}
\end{aligned}
$$

$$
\begin{aligned}
p_2 = -128(2(4\sigma^2 + (\mu_k z_1)^2)^2(1 + \frac{z_2^2}{\mu_k^2})^2 - 8\frac{X_0}{\mu_k^2}(4\sigma^2 \\
+ (\mu_k z_1)^2)(\frac{z_2^2}{\mu_k^2})((\mu_k z_1)^2 + 2\sigma(1 + 2\sigma + \frac{z_2^2}{\mu_k^2})) + \frac{X_0^4}{\mu_k^8}(3\frac{F_0^2}{\alpha^2\mu_k^4}(\frac{K_0}{L\mu_k^2} + \frac{K_{2R}}{L\mu_k^2} \\
+ \frac{2}{L\mu_k^2}(K_0 + K_{2R})\sigma + \frac{K_{2I}}{L\mu_k^2}(\mu_k z_1 + \frac{z_2}{\mu_k}))+ \\
2(1 + 4\sigma(1 + \sigma) + (\mu_k z_1 + \frac{z_2}{\mu_k})^2)^2) + \frac{X_0^2}{\mu_k^4}(192\sigma^3(1 + \frac{z_2^2}{\mu_k^2}) \\
+ 64\sigma^4(3 + \frac{z_2^2}{\mu_k^2}) + 12\sigma\mu_k z_1(\frac{F_0^2}{\alpha^2\mu_k^4}\frac{1}{L\mu_k^2}(K_{2I} \\
- K_{2R}\frac{z_2}{\mu_k}) + 4\mu_k z_1(1 + \frac{z_2^2}{\mu_k^2})) + 4\sigma^2(3\frac{F_0^2}{\alpha^2\mu_k^4} \\
\frac{1}{L\mu_k^2}(K_0 + K_{2R} + K_{2I}\frac{z_2}{\mu_k}) + 12(1 + \frac{z_2^2}{\mu_k^2})^2 + 8\mu_k z_1^2(3 + \frac{z_2^2}{\mu_k^2}) \\
+ 8\mu_k z_1(\frac{z_2}{\mu_k} + \frac{z_2^3}{\mu_k^3})) + (\mu_k z_1)^2(4 + 12(\mu_k z_1)^2 + 3\frac{F_0^2}{\alpha^2\mu_k^4 L\mu_k^2} \\
(K_0 - K_{2R} - K_{2I}\frac{z_2}{\mu_k}) + 4\frac{z_2}{\mu_k}(\mu_k z_1 + \frac{z_2}{\mu_k})(2 + \frac{z_2}{\mu_k}(\mu_k z_1 + \frac{z_2}{\mu_k})))) - \frac{X_0^3}{\mu_k^6}(128\sigma^4 \\
+ 64\sigma^3(3 + \frac{z_2^2}{\mu_k^2}) + 4\sigma^2(3\frac{F_0^2}{\alpha^2\mu_k^4 L\mu_k^2}(K_0 + K_{2R}) \\
+ 8(3 + 2\mu_k^2 z_1^2 + 2z_1 z_2 + 3\frac{z_2^2}{\mu_k^2})) + \mu_k z_1(8\mu_k z_1(1 + (\mu_k z_1 + \frac{z_2}{\mu_k})^2) \\
+ 3\frac{F_0^2}{\alpha^2\mu_k^4}(\frac{2K_{2I}}{L\mu_k^2} + \frac{K_0}{L\mu_k^2}\mu_k z_1 - K_{2R}(\mu_k z_1 + 2\frac{z_2}{\mu_k}))) \\
+ 4\sigma(3\frac{F_0^2}{\alpha^2\mu_k^4}(\frac{K_0}{L\mu_k^2} + \frac{K_{2R}}{L\mu_k^2} + \frac{K_{2I}}{L\mu_k^2}(\mu_k z_1 + \frac{z_2}{\mu_k}))+ \\
4((1 + \frac{z_2^2}{\mu_k^2})^2 + (\mu_k z_1)^2(3 + \frac{z_2^2}{\mu_k^2}) + 2\mu_k z_1(\frac{z_2}{\mu_k} + \frac{z_2^3}{\mu_k^3}))))) \quad \text{(E.12)}
\end{aligned}
$$

$$
\begin{aligned}
p_0 = 256\frac{F_0^2}{\alpha^2\mu_k^4}\frac{X_0^2}{\mu_k^4}((4\sigma^2 + (\mu_k z_1)^2)(1 + \frac{z_2^2}{\mu_k^2}) + \frac{X_0^2}{\mu_k^4}(1 + 4\sigma(1 + \sigma) \\
+ (\mu_k z_1 + \frac{z_2}{\mu_k})^2) - 2\frac{X_0}{\mu_k^2}((\mu_k z_1)^2 + 2\sigma(1 + 2\sigma + \frac{z_2^2}{\mu_k^2}))) \quad \text{(E.13)}
\end{aligned}
$$

Appendix F. Parameters of the equations of the singular points for a time-varying nonlinearity)

$$
\begin{aligned}
a_{sv} = \frac{-1}{256L\mu_k^2}\,[&18K_0K_{4I}\sin(4\delta_2) + 18K_0K_{4R}\cos(4\delta_2) \\
&+(-72K_{2I}K_{2r}\cos(2\delta_2) + 36K_{2I}K_{4R} - 36K_{2R}K_{4I} \\
&\quad +36K_0K_{2I})\sin(2\delta_2) \\
&+\left(36K_{2I}^2 - 36K_{2R}^2\right)\cos(2\delta_2)^2 + (-36K_{2R}K_{4R} \\
&\quad -36K_{2I}K_{4I} + 36K_0K_{2R})\cos(2\delta_2) \\
&\quad +9K_{4R}^2 + 9K_{4I}^2 + 36K_{2R}^2 - 27K_0^2]
\end{aligned}
\tag{F.1}
$$

$$
b_{sv} = \frac{-3}{16L\mu_k^2}\left(-1 + \frac{X_0}{\mu_k^2}\right)\left(K_{2R}\cos(2\delta_2) + K_{2I}\sin(2\delta_2) - K_0\right) \tag{F.2}
$$

$$
c_{sv} = \frac{z_2^2}{16\mu_k^2}\left(-1 + \frac{X_0}{\mu_k^2}\right)^2 \tag{F.3}
$$

References

[1] E. Shamonina, L. Solymar, Metamaterials: How the subject started, Metamaterials 1 (1) (2007) 12–18.

[2] G. Ma, P. Sheng, Acoustic metamaterials: From local resonances to broad horizons, Science Advances 2 (2016) e1501595.

[3] S. Tretyakov, A personal view on the origins and developments of the metamaterial concept, Journal of optics 19 (1) (2016) 013002.

[4] K. Fan, W. Padilla, Dynamic electromagnetic metamaterials, Materials Today 18 (1) (2015) 39–50.

[5] A. Urbas, Z. Jacob, L. Dal Negro, N. Engheta, A. Boardman, P. Egan, A. Khanikaev, V. Menon, M. Ferrera, N. Kinsey, et al., Roadmap on optical metamaterials, Journal of Optics 18 (9) (2016) 093005.

[6] M. Sato, B. E. Hubbard, A. J. Sievers, B. Ilic, D. A. Czaplewski, H. G. Craighead, Observation of locked intrinsic localized vibrational modes in a micromechanical oscillator array, Physical review letters 90 (4) (2003) 044102.

[7] M. Ruzzene, F. Scarpa, Directional and band-gap behavior of periodic auxetic lattices, physica status solidi (b) 242 (3) (2005) 665–680.

[8] M. Sato, B. E. Hubbard, A. J. Sievers, Colloquium: Nonlinear energy localization and its manipulation in micromechanical oscillator arrays, Reviews of Modern Physics 78 (1) (2006) 137.

[9] K. Bertoldi, P. Reis, S. Willshaw, T. Mullin, Negative poisson's ratio behavior induced by an elastic instability, Advanced materials 22 (3) (2010) 361–366.

[10] K. Bertoldi, V. Vitelli, J. Christensen, M. Van Hecke, Flexible mechanical metamaterials, Nature Reviews Materials 2 (11) (2017) 1–11.

[11] X. Yu, J. Zhou, H. Liang, Z. Jiang, L. Wu, Mechanical metamaterials associated with stiffness, rigidity and compressibility: A brief review, Progress in Materials Science 94 (2018) 114–173.

[12] J. Cha, C. Daraio, Electrical tuning of elastic wave propagation in nanomechanical lattices at mhz frequencies, Nature nanotechnology 13 (11) (2018) 1016–1020.

[13] S. Fischer, L. Hillen, C. Eberl, Mechanical metamaterials on the way from laboratory scale to industrial applications: Challenges for characterization and scalability, Materials 13 (16) (2020) 3605.

[14] G. Bordiga, L. Cabras, A. Piccolroaz, D. Bigoni, Dynamics of prestressed elastic lattices: homogenization, instabilities, and strain localization, Journal of the Mechanics and Physics of Solids 146 (2021) 104198.

[15] B. Lazarov, J. Jensen, Low-frequency band gaps in chains with attached non-linear oscillators, International Journal of Non-Linear Mechanics 42 (10) (2007) 1186–1193.

[16] A. Qureshi, B. Li, K. Tan, Numerical investigation of band gaps in 3d printed cantilever-in-mass metamaterials, Scientific Reports 6 (2016) 28314.

[17] M. Frazier, D. Kochmann, Band gap transmission in periodic bistable mechanical systems, Journal of Sound and Vibration 388 (2017) 315–326.

[18] A. Motcheyo, J. Macías-Díaz, Energy transmission in the forbidden band-gap of a nonlinear chain with global interactions, Journal of Physics A: Mathematical and Theoretical 53 (50) (2020) 505701.

[19] S. Ahmadisoleymani, S. Missoum, Optimization under uncertainty of a chain of nonlinear resonators using a field representation, Applied Mathematical Modelling 96 (2021) 779–795.

[20] S. Aubry, G. Kopidakis, A. M. Morgante, G. P. Tsironis, Analytic conditions for targeted energy transfer between nonlinear oscillators or discrete breathers, Physica B: Condensed Matter 296 (1-3) (2001) 222–236.

[21] G. Kopidakis, S. Aubry, G. P. Tsironis, Targeted energy transfer through discrete breathers in nonlinear systems, Physical Review Letters 87 (16) (2001) 165501.

[22] P. Panagopoulos, A. Vakakis, S. Tsakirtzis, Transient resonant interactions of finite linear chains with essentially nonlinear end attachments leading to passive energy pumping, International journal of solids and structures 41 (22-23) (2004) 6505–6528.

[23] R. Francesco, G. R., Wave propagation properties in oscillatory chains with cubic nonlinearities via nonlinear map approach, Chaos, Solitons & Fractals 27 (3) (2006) 606–617.

[24] L. Manevitch, New approach to beating phenomenon in coupled nonlinear oscillatory chains, Archive of Applied Mechanics 77 (5) (2007) 301–312.

[25] A. Ture Savadkoohi, C. Lamarque, J. Goutte, On the nonlinear interactions and existence of breathers in a chain of coupled pendulums, International Journal of Non-Linear Mechanics 94 (2017) 375–379.

[26] V. Settimi, M. Lepidi, A. Bacigalupo, Nonlinear dispersion properties of one-dimensional mechanical metamaterials with inertia amplification, International Journal of Mechanical Sciences 201 (2021) 106461.

[27] V. Settimi, M. Lepidi, A. Bacigalupo, Analytical spectral design of mechanical metamaterials with inertia amplification, Engineering Structures 274 (2023) 115054.

[28] K. Mikoshiba, J. Manimala, C. Sun, Energy harvesting using an array of multifunctional resonators, Journal of Intelligent Material Systems and Structures 24 (2) (2013) 168–179.

[29] R. Harne, M. Schoemaker, K. Wang, Multistable chain for ocean wave vibration energy harvesting, in: W.-H. Liao (Ed.), Active and Passive Smart Structures and Integrated Systems 2014, Vol. 9057, International Society for Optics and Photonics, SPIE, 2014, p. 90570B.

[30] D. Beli, A. Fabro, M. Ruzzene, J. Arruda, Wave attenuation and trapping in 3d printed cantilever-in-mass metamaterials with spatially correlated variability, Scientific Reports 9 (2019).

[31] V. Zega, P. Silva, M. Geers, V. Kouznetsova, Experimental proof of emergent subharmonic attenuation zones in a nonlinear locally resonant metamaterial, Scientific Reports 10 (2020) 12041.

[32] Y. Liu, Y. Wang, Vibration suppression of a linear oscillator by a chain of nonlinear vibration absorbers with geometrically nonlinear damping, Communications in Nonlinear Science and Numerical Simulation 118 (2023) 107016.

[33] G. Iooss, G. James, Localized waves in nonlinear oscillator chains, Chaos: An Interdisciplinary Journal of Nonlinear Science 15 (1) (2005) 015113.

[34] J. Flosi, C. Lamarque, A. Ture Savadkoohi, Different dynamics of a periodic mass-in-mass nonlinear chain during a single mode excitation, Meccanica 58 (1) (2023) 67–95.

[35] G. James, P. Kevrekidis, J. Cuevas, Breathers in oscillator chains with hertzian interactions, Physica D: Nonlinear Phenomena 251 (2013) 39–59.

[36] S. Charlemagne, A. Ture Savadkoohi, C. Lamarque, Dynamics of a linear system coupled to a chain of light nonlinear oscillators analyzed through a continuous approximation, Physica D: Nonlinear Phenomena 374 (2018) 10–20.

[37] G. James, Travelling breathers and solitary waves in strongly nonlinear lattices, Philosophical Transactions of the Royal Society A: Mathematical, Physical and Engineering Sciences 376 (2127) (2018) 20170138.

[38] A. Labetoulle, A. Ture Savadkoohi, E. Gourdon, Detection of different dynamics of two coupled oscillators including a time-dependent cubic nonlinearity, Acta Mechanica (2022) 1–32.

[39] A. Luongo, D. Zulli, Dynamic analysis of externally excited nes-controlled systems via a mixed multiple scale/harmonic balance algorithm, Nonlinear Dynamics 70 (2012) 1–13.

[40] A comparative study of the harmonic balance method and the orthogonal collocation method on stiff nonlinear systems, Journal of Sound and Vibration 333 (12) (2014) 2554–2567.

[41] A. Nayfeh, D. Mook, Nonlinear oscillations, 1995.

[42] L. Manevitch, The description of localized normal modes in a chain of nonlinear coupled oscillators using complex variables, Nonlinear Dynamics 25 (2001) 95–109.

[43] A. Luongo, D. Zulli, Dynamic analysis of externally excited nes-controlled systems via a mixed multiple scale/harmonic balance algorithm, Nonlinear Dynamics 70 (2012) 2049–2061.

[44] R. Bellet, B. Cochelin, P. Herzog, P. Mattei, Experimental study of targeted energy transfer from an acoustic system to a nonlinear membrane absorber, Journal of Sound and Vibration 329 (14) (2010) 2768–2791.

[45] O. Gendelman, Targeted energy transfer in systems with non-polynomial nonlinearity, Journal of Sound and Vibration 315 (3) (2008) 732–745.

[46] A. Ture Savadkoohi, C. Lamarque, Z. Dimitrijevic, Vibratory energy exchange between a linear and a nonsmooth system in the presence of the gravity, Nonlinear Dynamics 70 (2012) 1473–1483.

[47] Y. Starosvetsky, O. Gendelman, Strongly modulated response in forced 2dof oscillatory system with essential mass and potential asymmetry, Physica D: Nonlinear Phenomena 237 (13) (2008) 1719–1733.

[48] G. Hurel, A. Ture Savadkoohi, C. Lamarque, Nonlinear passive control of a pendulum submitted to base excitations, Acta Mechanica 232 (2021) 1583–1604.

[49] H. Poincaré, Les méthodes nouvelles de la mécanique céleste, Vol. 2, Gauthier-Villars et fils, imprimeurs-libraires, 1893.

[50] V. Guillot, A. Ture Savadkoohi, C. Lamarque, Tuning inter-modal energy exchanges of a nonlinear electromechanical beam by a nonlinear circuit, Archive of Applied Mechanics (2022).

[51] C. da Silveira Zanin, A. Labetoulle, E. De Bono, E. Gourdon, M. Collet, A. Ture Savadkoohi, Experimental evidences of nonlinear programmable electroacoustic loudspeaker, Building Acoustics 30 (3) (2023) 249–263.

[52] E. Boroson, S. Missoum, P. Mattei, C. Vergez, Optimization under uncertainty of parallel nonlinear energy sinks, Journal of Sound and Vibration 394 (2017) 451–464.